Structures in grain-refined directionally solidified hypoeutectic Al-Cu alloys: Benchmark experiments under microgravity on-board the International Space Station

G. Zimmermann, L. Sturz, C. Pickmann, E. Schaberger-Zimmermann, A. Roosz, A. Rónaföldi, Z. Veres, Ch.-A. Gandin, G. Reinhart, H. Nguyen-Thi, et al.

Structures in grain-refined directionally solidified hypoeutectic Al-Cu alloys: Benchmark experiments under microgravity on-board the International Space Station

G. Zimmermann [a,*], L. Sturz [a], C. Pickmann [a], E. Schaberger-Zimmermann [b], A. Roosz [c,d], A. Ronafoldi [c,d], Z. Veres [c,d], Ch.-A. Gandin [e], G. Reinhart [f], H. Nguyen-Thi [f], N. Mangelinck-Noël [f], Sh. McFadden [g], G.-U. Grün [h], W. Sillekens [i]

[a] ACCESS e.V., Intzestraße 5, 52072 Aachen, Germany

[b] Foundry Institut, RWTH Aachen University, Intzestraße 5, 52072 Aachen, Germany

[c] Institute of Physical Metallurgy, Metal Forming and Nanotechnology (UM), University of Miskolc, H3515 Miskolc, Hungary

[d] HUN-REN-ME Materials Science Research Group, 3515 Miskolc, Hungary

[e] Mines Paris – PSL, CEMEF CNRS UMR 7635, 06904 Sophia Antipolis, France

[f] Aix Marseille Univ, CNRS, IM2NP, Marseille, France

[g] School of Computing, Eng & Intel. Sys, Ulster University, Northern Ireland, UK Londonderry, United Kingdom

[h] Speira GmbH, Georg-von-Boeselager-Straße 21, 53117 Bonn, Germany

[i] European Space Agency – ESTEC, Keplerlaan 1 Postbus 299, 2200 AG Noordwijk, the Netherlands

Abstract

Benchmark solidification experiments were successfully performed under microgravity conditions on-board the International Space Station (ISS) within the ESAprogramme CETSOL (Columnar-to-Equiaxed Transition in SOLidification Processing). Cylindrical samples of grain-refined Al-4wt.%Cu, Al-10wt.%Cu and Al-20wt.%Cu alloys were directionally solidified in a gradient furnace to investigate columnar and equiaxed dendritic growth structures as well as the columnar to equiaxed transition under diffusive conditions.

The determination of temperature gradients; interface velocities; and cooling rates at liquidus, solidus, and eutectic front positions provides well-defined thermal experimental characterization. The evaluation of the flight samples demonstrates that no significant macrosegregation along the sample axis occurred and no radial effects were observed. Therefore, purely diffusive solidification behaviour without any residual melt convection can be assumed for these microgravity experiments. The analyses of the microstructure in longitudinal cross-sections show dendritic structures without any pore formation and the averaged eutectic fraction is largely constant along the sample. The samples of refined Al-4wt.%Cu alloy show a sharp CET from columnar dendrites to a fine equiaxed steady state grain structure whereas in the samples of refined Al-10wt.%Cu and Al-20wt.%Cu alloy, only equiaxed dendritic grain growth is observed. A quantitative analysis of the equiaxed grain morphology shows, that the shapes of the equiaxed dendrites depend on the applied temperature gradient, but the grain sizes in radial and longitudinal directions are identical. Therefore, a fully equiaxed dendritic growth structure without dendrite elongation was obtained. Compared to experiments in microgravity with non-refined Al-Cu alloys the average equiaxed grain size is about three times smaller.

Keywords: Dendritic solidification, Macrosegregation, Grain structure, Microstructure, Metal

1. Introduction

The properties of industrial casting products depend significantly on the microstructure, which is primarily the result of the solidification process conditions [1]. Binary hypoeutectic alloys typically solidify as a dendritic network surrounded by the eutectic phase. The features of the columnar or equiaxed dendritic grain structure, the average dendrite primary or secondary arm spacings and the percentage and distribution of the eutectic phase strongly affect the material properties. Therefore, a deep understanding of the formation of the microstructure and grain structure, as well as of the relationship with the solidification conditions, is essential to optimize the industrial processes and to verify the predictability of simulation tools.

On Earth, buoyancy-driven melt convection occurs in most castingsdue to thermal and solutal gradients in the melt that create local differencesin fluid density. Additionally, equiaxed dendritic grains may be advected by fluid flow or may float or sediment due to their buoyancy in the melt. Such transport processes also influence the evolution of columnar grains, the growth of equiaxed grains, and the columnar to equiaxed transition (CET) [2,3].

Here, solidification experiments under microgravity conditions can provide unique benchmark data by effectively suppressing the disturbing gravity-driven phenomena mentioned above. This allows for solidification conditions that are dominated by diffusion [4,5].

Within the ESA (European Space Agency) project CETSOL, directional solidification experiments have been carried out on selected aluminum-based alloys under microgravity conditions using the Material Science Laboratory (MSL) on-board the International Space Station (ISS). Previous microgravity experiments in the CETSOL project were conducted with Al-7wt.%Si alloy. The experiments used a decrease in temperature gradient or a sharp increase in pulling speed to trigger a CET in samples with and without grain refiner. Comparison of results from microgravity and terrestrial experiments enlightened the effects of gravity on the grain structure and on the CET. For Al-7wt.%Si alloy, it was shown that convective effects promote columnar growth by alleviating the blocking effects of equiaxed grains. The main results of these experiments were presented in detail in [6-14].

Those experiments provided important benchmark data for understanding the effect of gravity-driven transport on the CET. Meanwhile, these benchmark data for diffusive solidification of Al-7wt.%Si alloy were used to improve and verify several numerical models, describing the CET behavior quantitatively [11,15-18]. A so-called Concurrent Columnar Equiaxed Transition (C2ET) model was developed to predict results from microgravity solidification experiments that displayed both sharp and progressive columnar to equiaxed transitions. A clear objective of this C2ET model is to provide an alternative approach to a macroscale CET-model that does not require a specific blocking criterion (neither mechanical nor solutal blocking) but instead allows columnar and equiaxed grains to nucleate and grow concurrently according to the classic principles of real and phantom nucleation leading to extended growth (as used in the Kolmogorov approach to deriving the Avrami equation). Therefore, in contrast to other approaches, the C2ET model is a continuum method that predicts the microstructure characteristics at the macroscale of the casting. The C2ET approach produces results with reduced computational effort compared to models that model each crystal discretely. Along with the thermal histories, the microstructures of the four microgravity samples were simulated showing good agreement with experimental results [11,15]. Using a different approach and to better understand the impact of gravity on CET, directional solidification in Al-7wt.%Si alloy was simulated using the 3D CAFE model, with and without gravity [8,18]. The principle of the model is based on a time integration of nucleation and growth kinetics. The grains being nucleated, they concomitantly grow at the expense of the surrounding liquid and adopt elongated or round shapes as a function of their local environments, leading to columnar or equiaxed morphologies. Hence, as it is the case in the experiment, the final nature of the grains is not known

in advance with the CAFE model. It results from concurrent development of the grain boundaries from the melt, eventually leading to CET [8].

The simulations predicted the grain structure, temperature field and fluid velocity field in the melt. For the microgravity condition, diffusive transport was assumed. For the ground conditions with a solidification direction that was vertically upwards, the simulated melt convection propagated in the molten part of the sample - upward at the center and downward at the periphery. This phenomenon resulted in a longer propagation of the columnar structure at the center of the domain in the presence of gravity. The position of the CET is therefore predicted to be delayed in the ground simulation compared to the microgravity simulation. These findings agreed well with experimental results. Meanwhile, a 3D version of this code was implemented in the commercial software code THERCAST® at the company TRANSVALOR to be used in industrial processes.

To check the transferability of the knowledge gained from the microgravity experiments with Al-Si alloys to other metallic systems, hypoeutectic Al-Cu alloys are deemed to be suitable candidates. With addition of grain refiners (e.g. Titanium borides) such alloys are also model systems for high strength Al-based alloys. Additionally, for Al-Cu alloys with different Cu contents different density relations between Alrich fragments or equiaxed dendrites and the surrounding melt exist, which allows for the study of the effects related to flotation and sedimentation of fragments and unanchored equiaxed grains in the melt. It was shown [19] that in Al-Cu alloys with less than 10 wt.% Cu the primary solid is denser than the melt, while in alloys with more than 10 wt.% Cu the primary solid is less dense. Directional solidification in an upward manner on Earth results in a thermosolutally stable configuration in case of Al-4wt.%Cu alloy and in a thermosolutally unstable configuration with significant fragmentation and grain floatation in case of Al-20wt.%Cu alloy. For Al-10wt.% Cu alloy the density difference between the melt and primary Al solid is very low and convective melt flow is reduced but some fragmentations have been observed [20-23].

Nevertheless, experiments designed to be thermosolutally stable do not necessarily eliminate melt convection, and experiments using an alloy with a neutrally buoyant primary solid may still show some motion of unanchored dendritic grains in the melt [24]. In microgravity experiments, buoyancy-driven phenomena during solidification can be suppressed more effectively than by adjusting the composition [25].

Due to the density difference of Al-rich dendrites and Cu-enriched melt, X-ray diagnostics are often used to study the in-situ solidification behavior of Al-Cu alloys in thin, sheet-like samples of about 150-200 µm in thickness. Short-duration microgravity experiments were successfully performed during parabolic flight and sounding rocket missions. Columnar growth of non-refined Al-20wt.%Cu alloys was investigated to study the effect of intense fragmentation [22,23]. In Al-20wt.%Cu alloys, the nucleation behavior of

equiaxed dendrites ahead of the solidification front during CET was also investigated [26-30]. The same alloys were also used to analyze equiaxed dendritic growth in terrestrial gravity and in microgravity using isothermal cooling [31-33]. The output provided unique experimental data for validation of models of microstructural evolution of diffusion-controlled equiaxed alloy solidification [34,35]. Additional near-isothermal solidification experiments were carried out in Al-15wt.%Cu alloy to analyze the relationship between dendrite-boundary interaction and tip growth rates [36,37]. An overview on solidification of Al-Cu alloys was recently given in [38]. For the latter investigations, the duration of the microgravity period is about 20 s in parabolic flights and about 6 min in sounding rocket missions.

To achieve solidification of more relevant 3D bulk samples (that is, non-thin samples) as well as much longer microgravity durations, experiments on the ISS (or comparable orbiting platform) are needed. Recently, cylindrical samples of non-refined aluminum alloys containing 4, 10, and 18 wt.% copper were solidified upwards on Earth and in microgravity conditions aboard the ISS [39]. Even though all samples exhibited shrinkage pores of varying sizes, the microstructure, the eutectic fraction, the grain structure and the macrosegregation was analysed and the results are reported as benchmark data to validate future modeling efforts. A surprising outcome of these experiments was that all microgravity samples were entirely equiaxed, while the terrestrial samples exhibited a CET.

This present paper shows results of solidification experiments performed in microgravity on the ISS within the ESA MAP project CETSOL using cylindrical bulk samples of refined Al-Cu alloys. The Al-Cu samples contain 4, 10, or 20 wt.% Cu and were solidified in a BridgmanStockbarger type gradient furnace to investigate columnar and equiaxed dendritic growth as well as CET in purely diffusive conditions. The experiments reported herein thus complement previous investigations with Al-Cu alloys [39] using a different experimental set-up and investigations with Al-Si alloys [12] using a similar set-up (as well as complementing data from x-ray experiments on thin samples). The purpose of the paper is to comprehensively document the results of these reduced-gravity experiments, as a baseline or reference for comparison with other experimental and modeling works.

2. Alloy

Hypoeutectic aluminum-copper alloys are ideal candidates to study the development of columnar and equiaxed dendritic microstructures as a function of the Cu content. For the microgravity experiments presented in this paper Al-Cu alloys with 4 wt.%, 10 wt.% and 20 wt.% Cu were selected. To promote equiaxed growth in diffusive conditions all sample alloys contain 0.5 wt.% of master alloy AlTi5B for grain

refinement. AlTi5B alloys are the most common used aluminium grain refiners in aluminium alloys manufacturing to enhance mechanical properties of the alloy. The Al-Cu alloys were provided by Hydro Aluminum Rolled Products GmbH, now Speira GmbH, manufactored from high-purity Al and Cu material and delivered with certified measured compositions.

The alloy compositions were chosen to provide a useful range of copper addition levels over a meaningful range whilst remaining in the hypoeutectic range. It is well known that under terrestrial gravity conditions, binary aluminium alloys with less than 10 wt.% Cu solidify with initial solid that is sedimentary, whereas alloys with more than 10 wt.% Cu solidify with buoyant solid [19]. Alloys with 10 wt.% Cu are expected to nucleate solid with neutral buoyancy. In their benchmark experiments, Williams and Beckermann [39] choose 4, 10, and 18 wt.% Cu to promote different gravity-driven solid transport phenomena on earth that would then give clear distinction when tested under microgravity conditions (where gravity-driven transport effects are suppressed). Furthermore, as part of the XRMON project, Reinhart et al. [38] studied solidification with Al-20wt.% Cu under terrestrial and microgravity conditions using in-situ, X-ray analysis. In this current study, it was decided to use the compositions of 4 wt.%, 10 wt.% and 20 wt.% (with grain refiner added) in order to complement and compare against existing datasets from benchmark microgravity experiments from literature as meaningfully as possible, but with underpinning novelty in the furnace setup and cooling conditions applied.

3. Experiments

The microgravity experiments were performed in the MSL on-board the ISS. Six microgravity experiments have been conducted in a series named Batch 3a within the ESA MAP in the framework of the CETSOL project [6,40,41]. The measured gravity level has been better than 10^{-3}g during the stages of liquid processing of the samples at all times.

The six experiments were carried out using the Solidification and Quenching Furnace (SQF) insert of the MSL. The SQF and the sample cartridge assembly (SCA) are shown schematically in Fig. 1. The furnace consists of a hot and a cold zone separated by a so-called adiabatic zone. Typically, the cold zone is realized by a Liquid Metal Ring (LMR) to achieve a higher temperature gradient from the cold side and to allow for quenching. Here, the cold zone had the LMR function removed to achieve moderate temperature gradients up to about 4 K/mm, which were deemed sufficient to create conditions for CET. The hot zone is equipped with four heater zones H1-H4, which were adjusted to obtain the required temperature gradient, G, along the sample axis.

The metallic alloy samples (8 mm in diameter and 276 mm in length) were mounted inside a protective Al_2O_3 tubular crucible together with plugs made from the aluminum nitride material Shapal™ at both ends. The top end plug is conical to allow for expansion of the melt into the plug while heating and melting the alloy. Twelve N-type thermocouples (TC1-TC12) are located in four machined external axial grooves at the outer surface of the crucible to measure the temperature profile. The locations of the thermocouples as they relate to the zero-reference position of the SCA are also given in Fig. 1.

For each composition, two samples were used with different control parameters applied during stage-2 operation (as shown in Table 1).

Solidification of the alloy is performed by the controlled displacement of the SQF along the fixed SCA at a chosen velocity, which can be varied during the experiment. The position of the furnace at maximum melting position (x = 0 mm) relatively to the SCA is also given in Fig. 1. The furnace assembly was capable of translating to its end position at x = 150 mm.

The experimental procedure consists mainly of the heating-up and the solidification phase. In the heating-up phase the temperatures of all 4 heater zones of the SQF furnace were increased in several steps. The furnace was moved to the starting position x = 2 mm where the alloy was positioned almost fully in the heated zone. Finally, the heater temperatures of all 4 heater zones of the SQF furnace were adjusted to achieve the desired initial temperature gradient of G = 3◦C/mm in the region of the liquidus temperatures of the alloys. The final heater temperatures were 880◦C for samples 3#1 and 3#2, 850°C for samples 3#3 and 3#4, 830°C for sample 3#5 and 825°C for sample 3#6. These values were selected to be approximately 200◦C above the liquidus temperatures of the alloys (see Figs. 2 to 3, 4) and allowed for a moderate temperature gradient in the melt ahead of the solid-liquid interface. The direct experiment control was realized by the operational team at DLR/ MUSC with on-line contact to the experimenters. After reaching the final heater temperature settings, a homogenization time of about 30 to 40 min resulted in a stationary temperature profile inside the sample confirmed by the thermocouple measurements along the sample axis.

The solidification phase is described in three stages (see Table 1): In stage 1 furnace movement with the slowest velocity v_1 (0.005 mm/s) from furnace position x_1 to x_2. In stage 2 at position x_2, either the furnace velocity is increased by a factor of 10 to a value v2 (0.05 mm/s) or the temperatures of all heaters were decreased with cooling rate R and unchanged furnace velocity ($v_2 = v_1$). Faster movement of the furnace with v_3 (0.2 mm/s) until the end position x_4 = 150 mm completed the solidification phase in all cases. During this final stage 3, the temperature gradient and cooling rates are no longer controlled, but the temperature profile was still recorded.

These experimental parameters were defined within the CETSOL team and all experiments were successfully performed in the MSL on ISS in 2021 and afterwards returned with SpaceX-22 and SpaceX-23 space crafts to Earth. De-integration of the SCA cartridges was performed by Soterem in Toulouse, France, and the processed samples - still integrated in the Al_2O_3 crucible - were delivered to Access e.V. for further microstructure analysis.

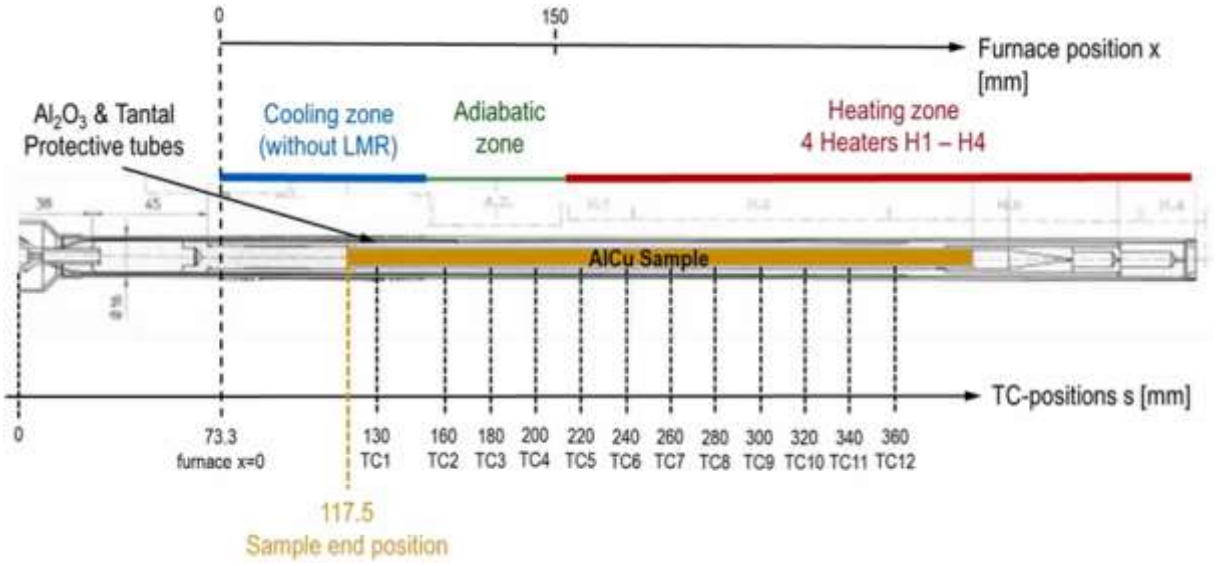

Fig. 1. Schematic setup of the SCA inserted in the SQF of the MSL on-board the ISS. The SCA contains the Al–Cu alloy inserted as a cylinder of 8 mm diameter and 276 mm length. The SQF is shown schematically at its initial position with respect to the SCA. It moves to the right during the solidification experiment. The positions of the 12 thermocouples TC1 to TC12, are distributed evenly along the sample.

Table 1. Control parameters for the six CETSOL solidification experiments performed under microgravity: Notation g.r. means grain refined alloys containing 0.5 wt.% of master alloy AlTi5B. Generally, the furnace pulling velocity is denoted as v_n within the respective operating stage n (where n = 1,2, or 3). The range of motion for a given stage n is given as xn-xn+1 over which the pulling speed vn is applied. R is the applied cooling rate of all 4 heater zones in stage 2.

Sample	Alloy	Initial G, K/mm	Stage 1		Stage 2			Stage 3	
			v_1,	x_1_x_2, mm	v_2,	x_2-x_3, mm	R, K/min	v_3,	x_3-x_4, mm
mm/s					mm/s				mm/s
3#1	Al-4wt.%Cu, g.r.	3	0.005	2– 30	0.050	30–80	0	0.200	80–150
3#2		3	0.005	2–30	0.005	30–61	5	0.200	61–150
3#3	Al-10wt.%Cu, g.r.	3	0.005	2–40	0.050	40–90	0	0.200	90–150
3#4		3	0.005	2–40	0.005	40–67	5	0.200	67–150
3#5	Al-20wt.%Cu, g.r.	3	0.002	2–30	0.020	30–80	0	0.200	80–150
3#6		3	0.002	2–30	0.002	30–50	2	0.200	50–150

4. Microstructure analysis

Before microstructure analysis was performed on radial and longitudinal cross-sections, relevant parts of the samples (from the partly melted region upon starting the solidification experiment to the end of solidification stage 2) were analysed using a computer tomograph (CT). The density difference between Al-rich dendrites and the residual Curich eutectic phase of the Al-Cu alloys allows for identification of the microstructure in 3D with a spatial resolution of about 15 μm. This nondestructive method demonstrated that no pores larger than the resolution of CT scan existed in the processed samples. Additionally, regions with different microstructures like the TGZM-influenced region (temperature gradient zone melting), columnar or equiaxed dendrites can be identified clearly. Video sequences of such CT measurements in top view were obtained by frame-by-frame animation of the CT sections in the sample volume and are given as supplementary material. These sequences can be considered as benchmark data for full 3D simulations.

As regards metallographic analyses, the solidified samples were cut into parts of 30 mm in lengths. The cutting positions were informed by the CT scans to avoid the possibility of cutting through any potential CET regions. The microstructure and grain structure in the axial cross-sections were characterized with this procedure. Optical micrographs from selected radial cross-sections are given in the supplementary materials and can be compared to the CT videos.

In a follow-up step, the 30 mm sample pieces were cut lengthwise close to the center line into two halves and used for further analysis along the longitudinal direction. Mechanical polishing with diamond suspension was used to help reveal the dendritic structures through optical microscopy (OM).

To determine the eutectic fraction (f_{eut}) the grey-scale images of the longitudinal cross-sections (30 mm × 8 mm) were subdivided into boxes of size 0.4 mm × 0.4 mm. The size of these boxes was chosen close to the size of the equiaxed dendritic grain structure formed during stage 2. It is thus smaller than the primary dendrite arm spacing in the columnar region and systematically includes a mixture of the dendritic and eutectic microstructures. For each of these boxes an identical grey level threshold was set to count the number of pixels related to the dendritic phase appearing in white and the residual number of pixels for the heterogeneous eutectic phase (dark phase). In each of the samples 3#3 and 3#4 one region shows a surface defect resulting from a shrinkage pore. The boxes inside these regions were removed manually before further evaluation. Taking the average of the proportion of eutectic phase for all these

evaluable boxes resulted in a mean overall average eutectic fraction for the whole sample. In an iteration process, the grey value threshold was adapted such that this average eutectic fraction for the whole sample corresponds to the values given by the Scheil model [1] for each alloy composition, where f_{eut} Scheil = 0.0916 for Al-4wt.% Cu, f_{eut} Scheil = 0.2547 for Al-10wt.%Cu and f_{eut} Scheil = 0.4928 for Al-20wt.%Cu. This methodology was also used in [35] and allowed for the evaluation of relative variations of the eutectic fraction along the sample sufficiently well. The results of the eutectic measurements are graphically represented into 2D maps. Additionally, the eutectic fraction results are averaged in the radial direction to create averaged profiles of f_{eut} along the sample axis. To eliminate potential effect of grey level error at the edge of the sample, the first and the last of the 20 boxes in radial direction were not included for this evaluation.

To characterize the grain structure, the longitudinal cross-sections are electrolytically etched using Barker's reagent [42]. Observation with a polarized optical microscopy produced color contrast based on the different grain orientations to identify different dendritic grains. The grain size was then determined using a simple intercept method, where lines were superimposed across the diameter (sample width) at regular intervals of 0.8 mm along the sample axis. The number of grain boundary intercepts on each line was counted manually. The radial mean intercept length (RMIL) is then reported as the length of each line divided by the number of grain boundary intersections with that line. While the RMIL should not be taken as a true grain size, it characterizes grain size changes along the axis approximately [39].

5. Results

5.1. Cooling curves

Measured temperatures of thermocouples TC1 to TC12 for all experiments as well as the furnace position x (see Fig. 1) are shown in Figs. 2 to 4. Time is labelled such that the solidification stage 1 is shown to begin at t = 0 s. Liquidus, solidus and eutectic isotherms of the alloy are indicated with black horizontal dashed lines. According to the Al-Cu phase diagram [43,44], the liquidus temperature of the alloy decreases with increasing Cu content. The different solidification stages 1 to 3 are marked by dashed vertical lines. The temperature curves of all samples indicate that nominal sample processing was achieved.

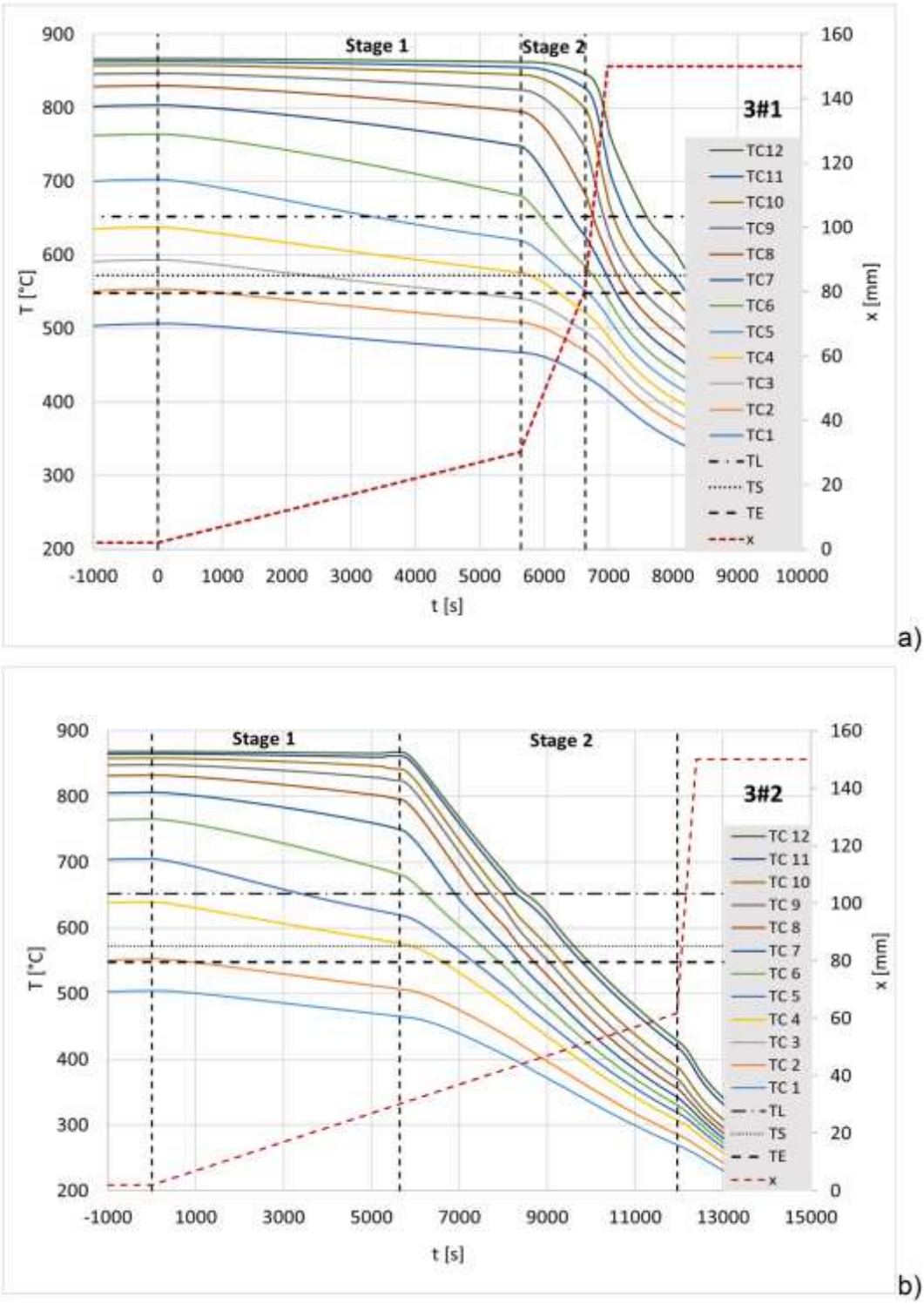

Fig. 2. Recorded temperature curves at thermocouple positions TC1 to TC12 and furnace position x (Fig. 1) for a) sample 3#1 and b) sample 3#2. The solidification stage 1 begins at t = 0 s. Liquidus, solidus and eutectic isotherms of the Al-4wt.%Cu alloy (T_L = 652°C, T_S = 572°C and T_E= 548°C [44]) are indicated with black horizontal dashed lines. The solidification stages are marked by dashed vertical lines. The red dashed line corresponds to the position of the furnace.

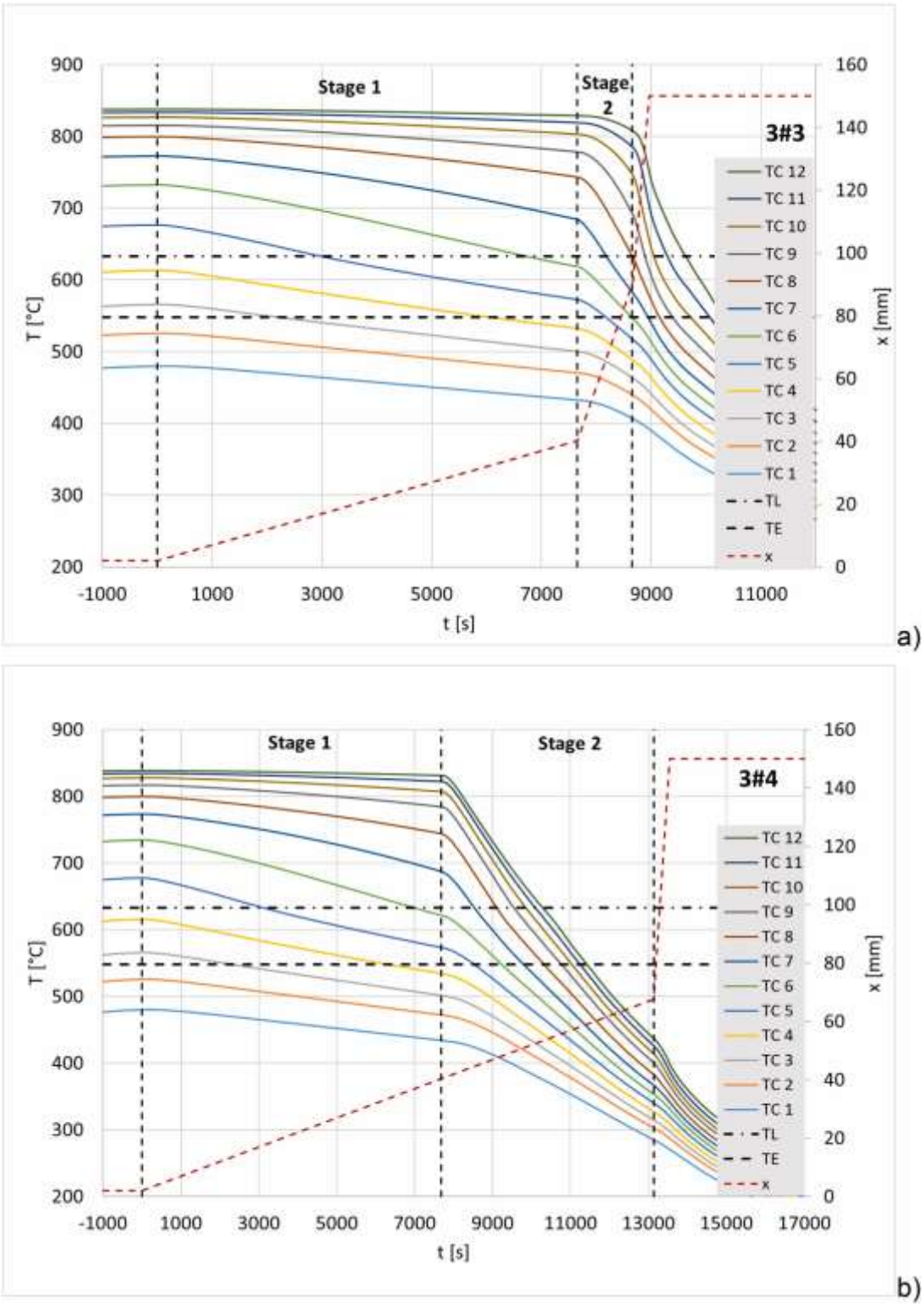

Fig. 3. Recorded temperature curves at thermocouple positions TC1 to TC12 and furnace position x (Fig. 1) for a) sample 3#3 and b) sample 3#4. The solidification stage 1 begins at t = 0 s. Liquidus and eutectic isotherms of the Al-10wt.%Cu alloy (TL = 633◦C and TE= 548◦C [44]) are indicated with black horizontal dashed lines. The solidification stages are marked by dashed vertical lines. The red dashed line corresponds to the position of the furnace.

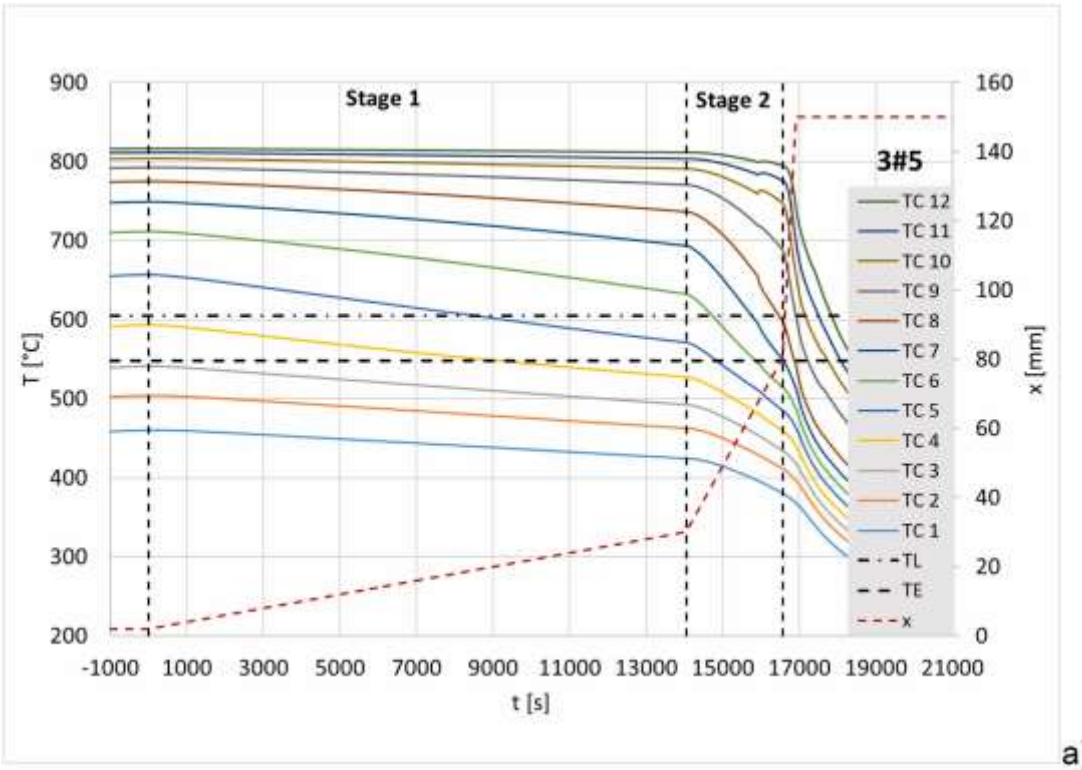

a)

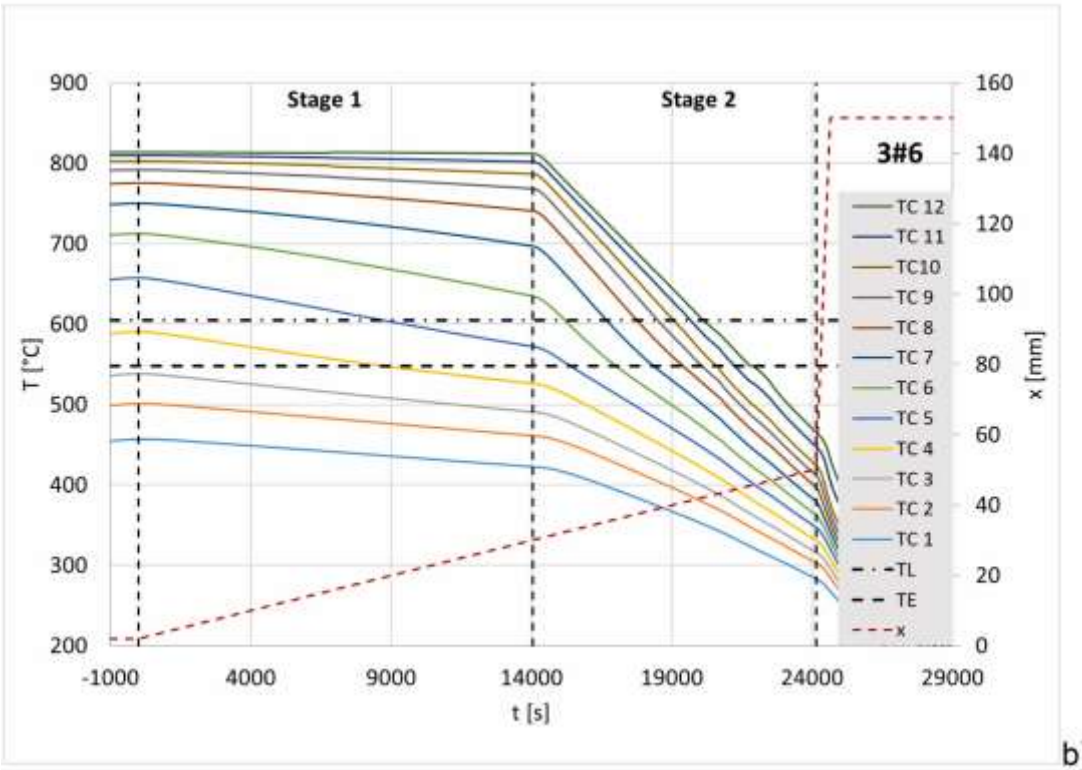

b)

Fig. 4. Recorded temperature curves at thermocouple positions TC1 to TC12 and furnace position x (Fig. 1) for a) sample 3#5 and b) sample 3#6. The solidification stage 1 begins at t = 0 s. Liquidus and eutectic isotherms of the Al-20wt.%Cu alloy (TL = 605◦C and TE= 548◦C [44]) are indicated with black horizontal dashed lines. The solidification stages are marked by dashed vertical lines. The red dashed line corresponds to the position of the furnace.

5.2. Local solidification velocities and temperature gradients

Assuming a negligible undercooling of both the primary dendrite tips solidification process of the samples can be characterized by the isotherm velocities (vL and vE) and the temperature gradients (G_L and G_E) of the solid/liquid (S/L) and eutectic/liquid (E/L) isotherms as a function of time. From the TC1 to TC12 temperature data for each time and the eutectic front, solidification starts at the liquidus temperature (T_L) and is completed when the eutectic temperature (T_E) is reached. Therefore, the step a high order polynomial function (typically 6–10 order) was used to fit the temperature–sample T(s) positions at every time step with an accuracy higher than $R_2 > 0.999999$. From all these T(s) functions, the positions of liquidus and eutectic isotherms (x_L and x_E) were determined at $T=T_L$ and $T=T_E$ temperatures. Here again, a 6–10 order polynomic function was used to fit these data sets ($x_L(t)$ and $x_E(t)$ functions) with an accuracy higher than R2 > 0.999999. The time derivatives of these position values for the isotherms are assumed to provide the corresponding liquidus and eutectic velocities (v_L and v_E) as a function of the sample position. Additionally, the local axial temperature gradients along the sample axis (G_L and G_E) ahead of the corresponding temperatures were calculated, as well as the local cooling rates R ($R_L = G_L v_L$ and $R_E = G_E v_E$). For the sake of completeness, in case of Al-4wt.%Cu alloy [39], the values at the solidus temperature (G_S, v_S and R_S) were also calculated. More details of the analyses are given in [45].

The local values at eutectic temperature were used to check and confirm the location of the maximum melting position in the processed samples but are not given here. The local values at liquidus temperature presented in the following results are assumed to describe the situation close to the dendrite tips in the case of columnar solidification or for equiaxed dendrites nucleating close to the solidification front.

5.3. Evaluation of the microstructure

Figs. 5 to 10 summarize the microstructure and thermal evaluation of the µg samples CETSOL 3#1 to 3#6. The processing parameters (velocity of the liquidus isotherm v_L, temperature gradient ahead of the liquidus isotherm GL, furnace velocity v_F and cooling rate at liquidus isotherm R_L), together with the full microstructure and eutectic fraction evaluation (averaged eutectic fraction feut, eutectic fraction obtained from the Scheil model f_{eut} Scheil, grain structure, and R_{MIL} profile representing the grain size as a function of the sample positions) are gathered on these figures. The given section ranges from the partly melted region

upon starting the solidification experiment to the end of solidification stage 2. High quality images of the cross-sections are given in the supplementary materials.

The evaluation of the velocity of the liquidus isotherm v_L shows that in all experiments, the nominal value for stage 1 (see Table 1) is reached rather soon and then remains constant. In stage 2, in the cases of a sudden increase of the furnace velocity (Figs. 5, 7 & 9), the velocity of the liquidus isotherm v_L follows the furnace velocity but with a delay.

Sample CETSOL3#3 shows some localised specific behaviour (velocity, eutectic percentage, grain size) at about s = 270 mm, which is attributed to a surface pore (Fig. 7). The formation of such a shrinkage pore may influence the microstructure by inducing a liquid flow by the pore expansion and Marangoni effect [9]. CETSOL3#5 shows an increase in v_L after axial position s = 280 mm probably caused by the separation into two parts of the solidifying sample at s = 290.5 mm (Fig. 9). In the cases with a decrease of the heater temperatures at unchanged furnace velocity (Figs. 6, 8 & 10), the velocity of the liquidus isotherm v_L shows a continuous increase as expected. The analysis of the thermal data also shows that in the solidification stage 1 a temperature gradient ahead of the liquidus isotherm GL between 3.0 K/mm and 3.5 K/mm was achieved, which is close to the nominal value. In case of a sudden increase of the furnace velocity, G_L in stage 2 decreased only slightly (Figs. 5, 7 & 9). For experiments 3#2, 3#4 and 3#6 (Figs. 6, 8 & 10), for which a cooling rate is applied during stage 2 by decreasing the temperature of the heaters, a continuous decrease of the liquidus isotherm temperature gradient GL is shown. It differs from experiments 3#1, 3#3 and 3#5 (Figs. 5, 7 & 9) for which a sharp decrease was induced by the velocity change of the furnace (Table 1). The longitudinal cross-sections in Figs. 5 to 10 show dendritic structures without any pore formation inside the processed alloy in the sections of interest. In general, in the partly melted region (present upon starting the solidification experiment) the amount of eutectic fraction is reduced. This may be explained by some temperature gradient zone melting (TGZM) effect during the thermal homogenization phase before starting the solidification stage 1 [46-48]. Besides this initial effect, the averaged eutectic fraction f_{eut} is globaly quite constant along the sample. This confirms a diffusive solidification behavior with negligible macrosegregation along the sample axis. The samples 3#1 and 3#2 with Al-4 wt.% Cu alloy show columnar grain structure in stage 1 (Figs. 5 & 6) with just a few grains, followed by an equiaxed grain structure in stage 2. For these low Cu composition samples, a clear columnar-to-equiaxed transition is detectable. For each of the two higher Cu-composition samples (Al-10 wt.% Cu and Al-20 wt. % Cu), equiaxed dendritic grain growth is observed directly in stage 1 (Figs. 7 to 10). The grain size given in the

R_{MIL} plots is dramatically reduced in stage 2 in all samples. In samples 3#3 and 3#4 with Al-10 wt.% Cu alloy, a large surface pore is detected close to the end of solidification stage 2 (Figs. 7 & 8).

In sample 3#3 the interface velocity v_L, the R_{MIL} value as well as the eutectic fraction f_{eut} show a locally limited decrease. Therefore, this pore formation has a local impact on the microstructure and grain structure, but does not change the general evolution [9]. Table 2 summarizes the stationary values of the grain size R_{MIL} in stages 1 & 2 as a function of the process parameters for the flight samples.

The analysis of the R_{MIL} values shows that the changes of the process parameters between stage 1 and stage 2 triggered a sharp CET for samples 3#1 & 3#2 (low Cu content) and result in the establishment of a fine grain structure that developed rapidly. Within a solidification length of about 2 mm to 6 mm a fully equiaxed, steady-state dendritic grain structure is observed.

This evaluation of the flight samples demonstrated that no significant macrosegregation occurred along the sample axis. Also, no radial effects, for example, caused by a potential radial temperature gradient in the grain structure can be observed. Therefore, a pure diffusive solidification behavior without any residual melt convection can be reasonably assumed for the microgravity experiments, as expected. Even when the velocity of the liquidus isotherm v_L increased, the temperature gradient ahead of the liquidus isotherm, G_L, decreased with the result that the mean local cooling rate R_L is comparable to the case of the experiments with furnace velocity increase (see Table 2). As a consequence, the R_{MIL} values in stage 2 are also comparable for samples with the same Cu content.

The experiments were performed in an axial temperature gradient of about 3 K/mm, which may have affected the shape or elongation of the equiaxed dendrites [49]. Fig. 11 shows select, detailed micrographs of the electrolytically etched cross-sections (height by width = 2.10 mm by 2.65 mm) of microgravity samples CETSOL 3#1, 3#3 and 3#5. A set of such images for all samples is given in the supplementary materials. The images show the equiaxed grain structure in longitudinal cross-sections with growth direction from left to right, and in radial cross-section for alloys with different Cu compositions and process parameters. In the Al-4wt.%Cu alloy, the grain structure shows no noticeable difference between longitudinal and radial cross-sections. The equiaxed dendrites in Al-10wt.%Cu and Al-20wt.%Cu alloys display

significant forced growth of dendrite arms along the axial temperature gradient in the longitudinal cross-sections.

For quantitative evaluation of the grain size, the R_{MIL} was also determined in the radial cross-sections. Similar to the evaluation of R_{MIL} in longitudinal cross-sections, a line structure with distances of 0.8 mm was superimposed and the number of intercepts was counted to calculate R_{MIL} radial. Fig. 12 shows the steady-state values of both R_{MIL} and R_{MIL} radial as a function of the averaged local cooling rate R_L in the stages 1 & 2. Despite the apparent variation in shapes of the equiaxed dendrites in longitudinal and radial directions, the R_{MIL} values agree quite well within the assumed error of about 5%. Therefore, it can be considered that fully equiaxed dendritic growth with negligible elongated dendrites are present. In case of equiaxed grains, the grain size depends on the conditions of both nucleation and growth. Only the latter being explicitly dependent on the cooling rate, while the nucleation is strongly affected by the number of refiners acting as nucleation sites and their positions, which also depend on the solute profile ahead the existing layer of equiaxed grains. For Al-alloys, it is shown that the equiaxed grain size depends on the cooling rate like $\lambda = A\, R^{-n}$ [50]. The fit of all R_{MIL} values of equiaxed growth results in A = 0.148 and n= 0.3592 ± 0.0222, which is close to the value n = 0.27 for non-refined Al-4.3wt.%Cu alloy [50].

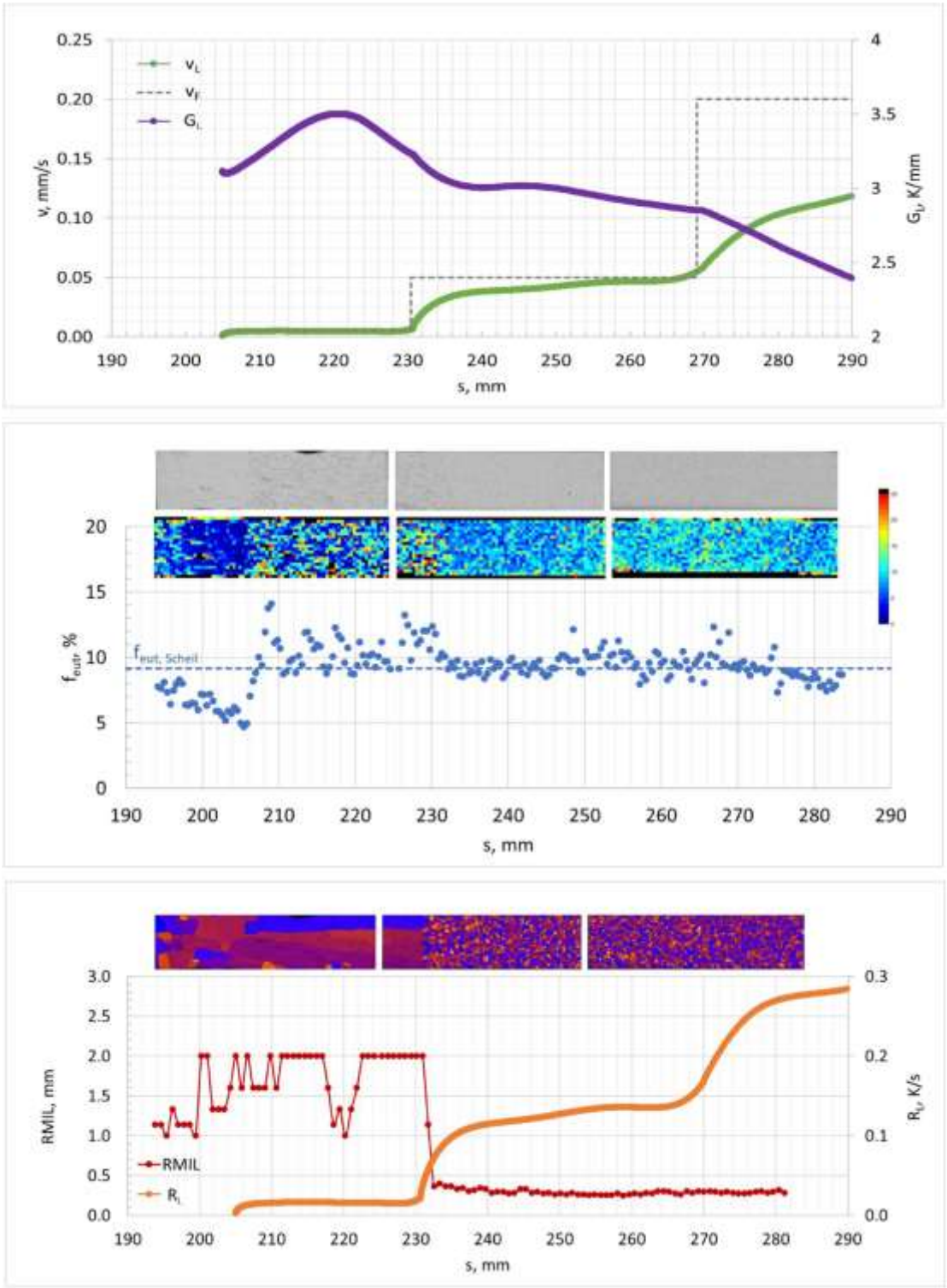

Fig. 5. Furnace velocity v_F, velocity of the liquidus isotherm v_L and temperature gradient ahead of the liquidus isotherm G_L (top), microstructure, eutectic fraction map, the axial profile of diameter averaged eutectic fraction feut and the value obtained from the Scheil model f_{eut} Scheil (middle), micrographs of the electrolytically etched longitudinal cross-sections showing the grain structure and the R_{MIL} profile representing the grain size together with the cooling rate at liquidus isotherm R_L (bottom) for the Al-4wt.%Cu sample CETSOL 3#1.

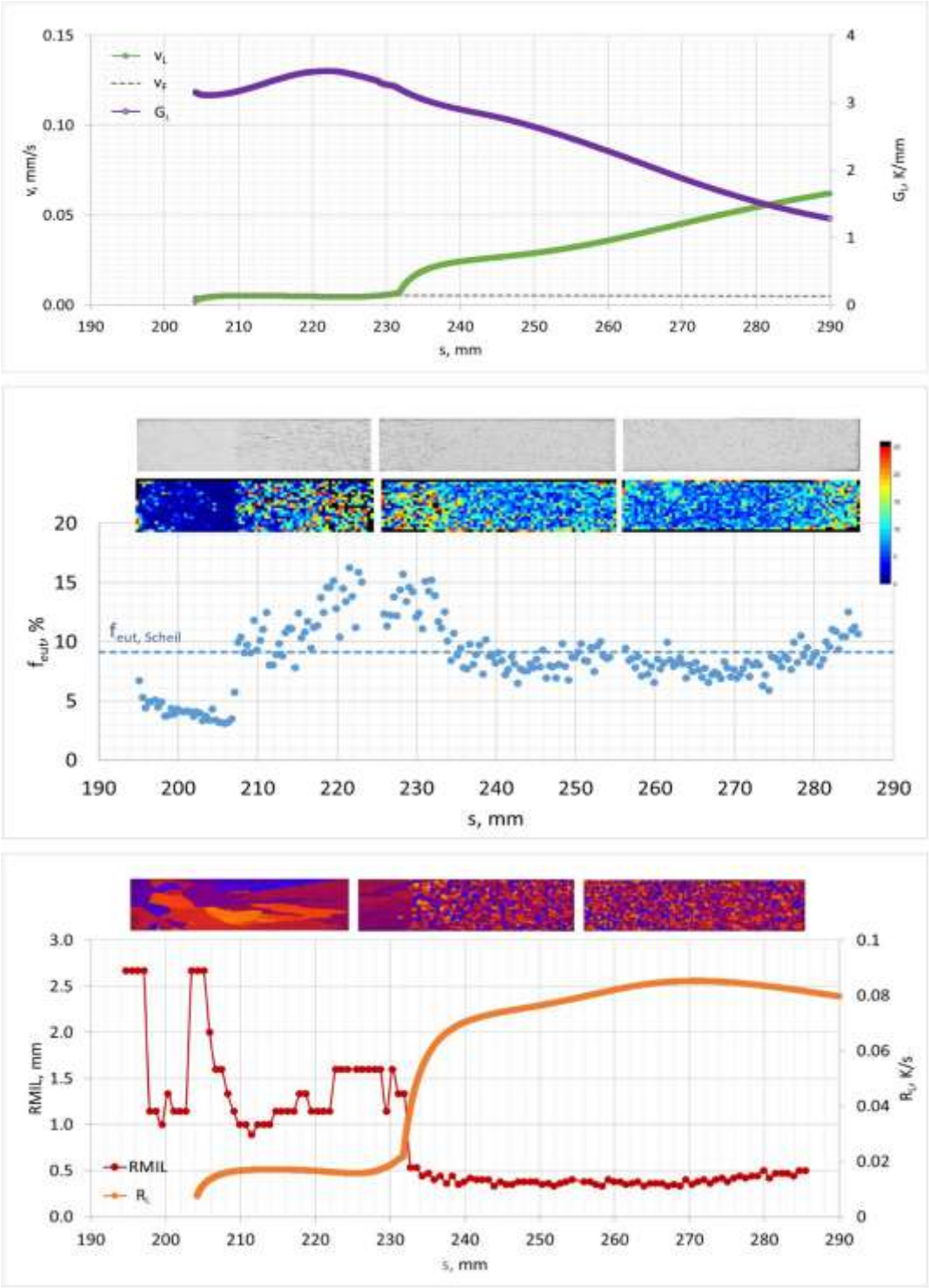

Fig. 6. Furnace velocity v_F, velocity of the liquidus isotherm v_L and temperature gradient ahead of the liquidus isotherm G_L (top), microstructure, eutectic fraction map, the axial profile of diameter averaged eutectic fraction f_{eut} and the value obtained from the Scheil model f_{eu}t Scheil (middle), micrographs of the electrolytically etched longitudinal cross-sections showing the grain structure and the R_{MIL} profile representing the grain size together with the cooling rate at liquidus isotherm R_L (bottom) for the Al-4wt.%Cu sample CETSOL 3#2.

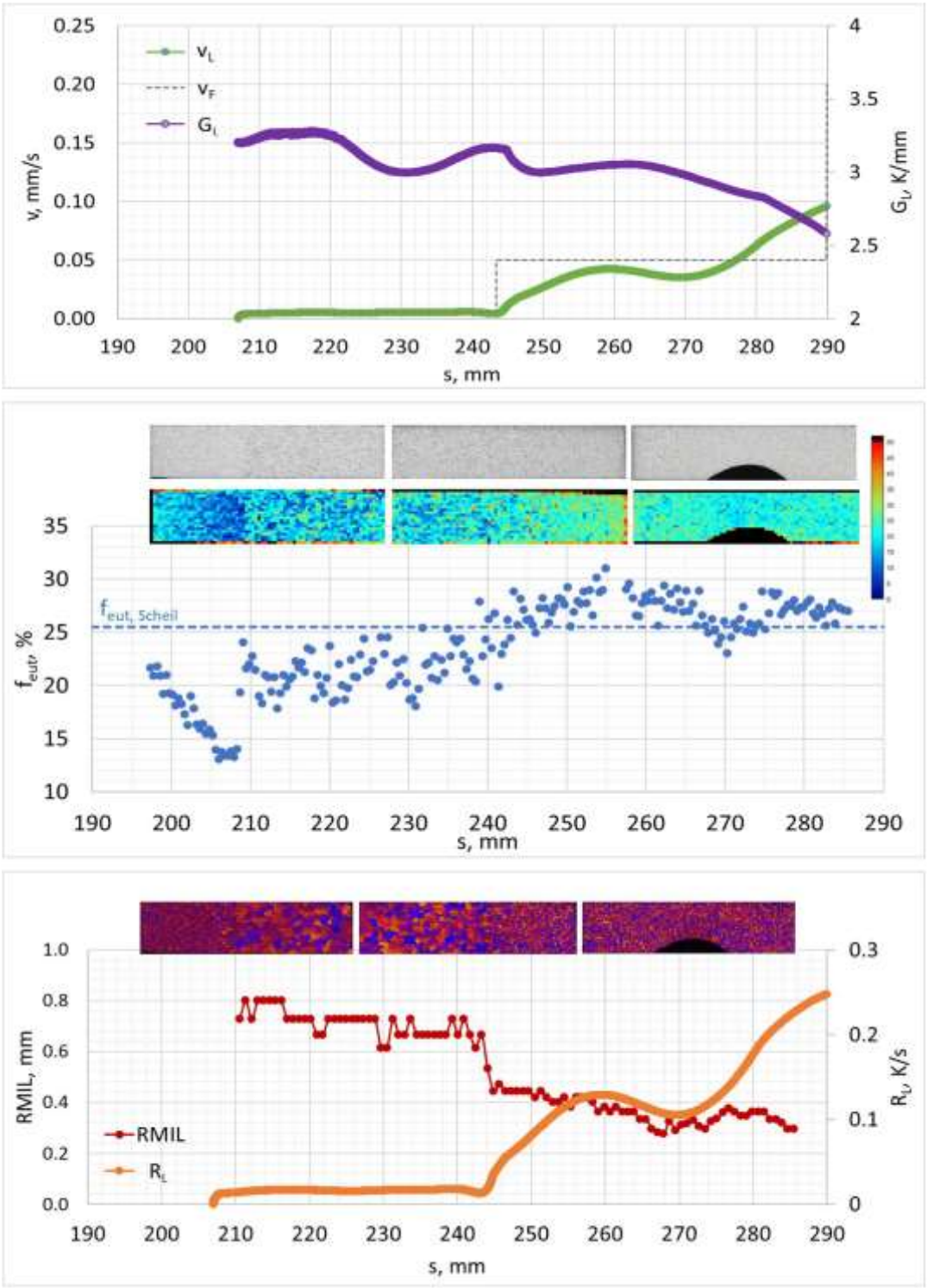

Fig. 7. Furnace velocity v_F, velocity of the liquidus isotherm v_L and temperature gradient ahead of the liquidus isotherm G_L (top), microstructure, eutectic fraction map, the axial profile of diameter averaged eutectic fraction f_{eut} and the value obtained from the Scheil model f_{eut} Scheil (middle), micrographs of the electrolytically etched longitudinal cross-sections showing the grain structure and the R_{MIL} profile representing the grain size together with the cooling rate at liquidus isotherm R_L (bottom) for the Al-10wt.%Cu sample CETSOL 3#3.

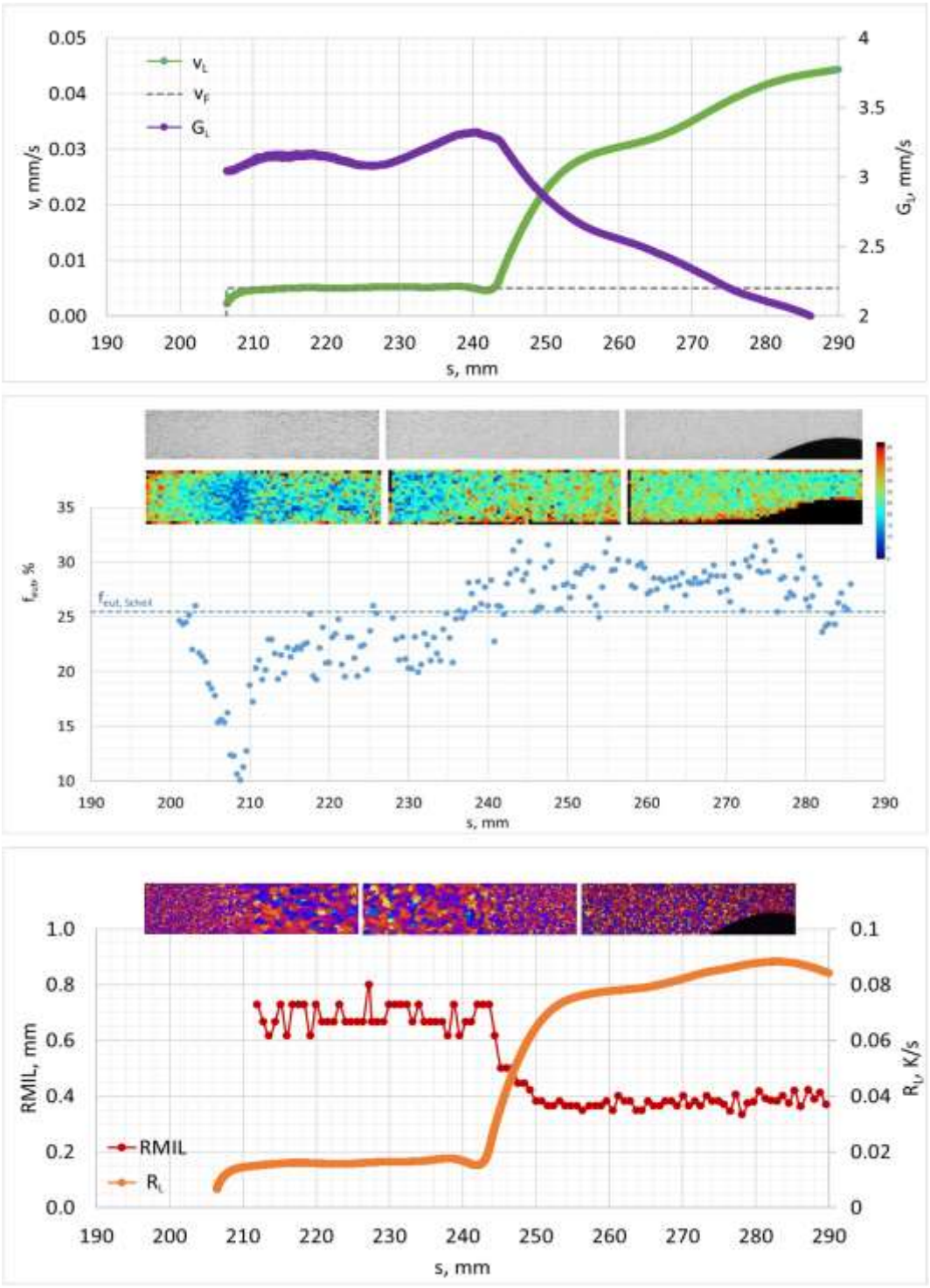

Fig. 8. Furnace velocity v_F, velocity of the liquidus isotherm v_L and temperature gradient ahead of the liquidus isotherm G_L (top), microstructure, eutectic fraction map, the axial profile of diameter averaged eutectic fraction f_{eut} and the value obtained from the Scheil model f_{eut} Scheil (middle), micrographs of the electrolytically etched longitudinal cross-sections showing the grain structure and the R_{MIL} profile representing the grain size together with the cooling rate at liquidus isotherm R_L (bottom) for the Al-10wt.%Cu sample CETSOL 3#4.

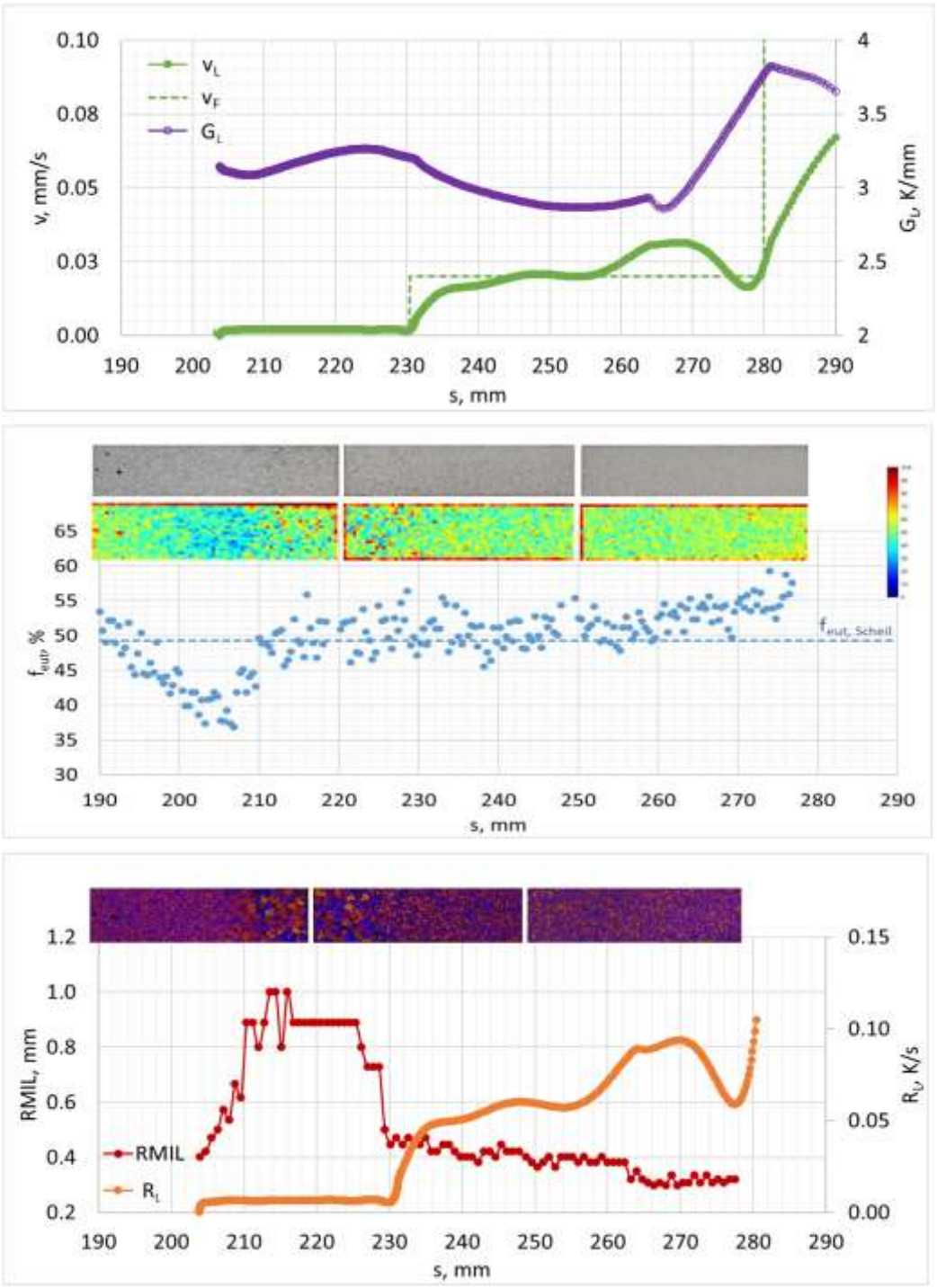

Fig. 9. Furnace velocity v_F, velocity of the liquidus isotherm v_L and temperature gradient ahead of the liquidus isotherm G_L (top), microstructure, eutectic fraction map, the axial profile of diameter averaged eutectic fraction f_{eut} and the value obtained from the Scheil model f_{eut} Scheil (middle),micrographs of the electrolytically etched longitudinal cross-sections showing the grain structure and the R_{MIL} profile representing the grain size together with the cooling rate at liquidus isotherm R_L (bottom) for the Al-20wt.%Cu sample CETSOL 3#5.

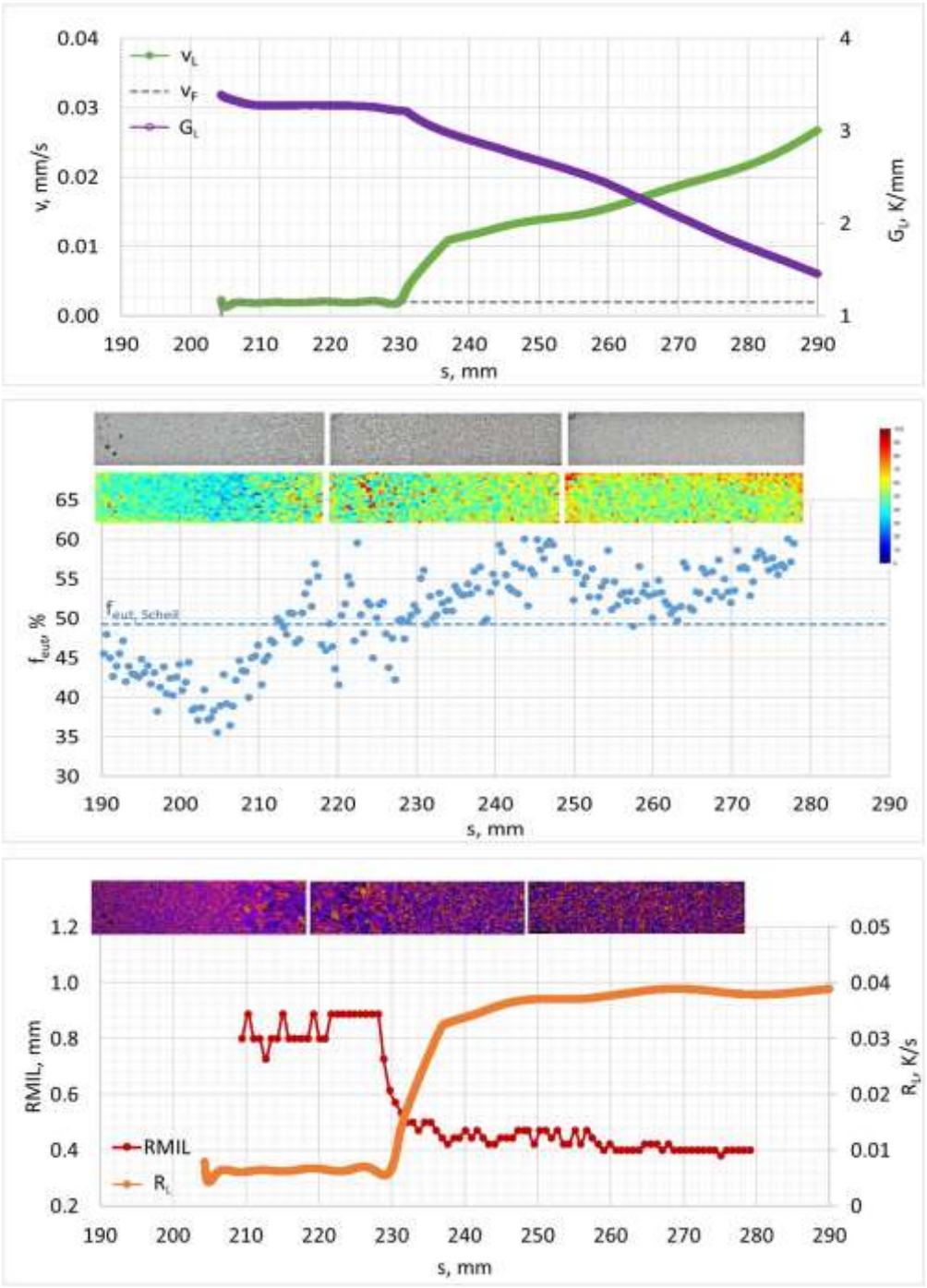

Fig. 10. Furnace velocity v_F, velocity of the liquidus isotherm v_L and temperature gradient ahead of the liquidus isotherm G_L (top), microstructure, eutectic fraction map, the axial profile of diameter averaged eutectic fraction f_{eut} and the value obtained from the Scheil model f_{eut} Scheil (middle), micrographs of the electrolytically etched longitudinal cross-sections showing the grain structure and the R_{MIL} profile representing the grain size together with the cooling rate at liquidus isotherm R_L (bottom) for the Al-20wt.%Cu sample CETSOL 3#6.

Table 2. Averaged local cooling rate RL, radial mean intercept length RMIL and averaged number of grains in radial direction Nrad in solidification stages 1 & 2 for the six CETSOL samples solidified under microgravity.

Sample	Alloy	Stage 1			Stage 2		
		R_L, K/s	RMIL, mm	Nrad	R_L, K/ s	RMIL, mm	Nrad
3#1	Al-4wt.% Cu, g.r.	0.015 0.016	2.0 1.6	4	0.11 0.07	0.35 0.40	23
3#2				5			20
3#3	Al-10wt.% Cu, g.r.	0.0175 0.0163	0.7	11	0.125 0.077	0.40 0.36	20
3#4			0.67	12			22
3#5	Al-20wt.% Cu, g.r.	0.007	0.89	9	0.05	0.42	19
3#6		0.006	0.89	9	0.036	0.44	18

5.4. Comparison with microgravity experiments in non-refined AlCu alloys, Ref. [39]

Williams and Beckermann [39] solidified cylindrical samples of three non-refined Al-Cu alloys (Al-4wt.%Cu, Al-10wt.%Cu and Al-18wt. %Cu) in microgravity environment on the ISS and on Earth. In the following, the results of the space-grown samples are compared to those of CETSOL samples 3#1, 3#3 and 3#5 (Al-4wt.%Cu, Al-10wt.%Cu and Al-20wt.%Cu) given in this paper.

The alloy compositions are comparable although all CETSOL sample alloys also contain 0.5 wt.% of master alloy AlTi5B for grain refinement. The sample dimensions in [39] are 9 mm in diameter and 60 mm in length, compared to 8 mm in diameter and 276 mm in length for the CETSOL sample. Volume compensation during melting and solidification in [39] was realized by an active spring system, and by a passive volume compensation device in the MSL cartridges (Fig. 1). The SUBSA furnace used in [39] consisted of one heater and passive cooling with a fixed sample position. Solidification in all experiments was realized using a power-down technique by applying the same constant cooling rate of 5◦C/min to the heater. The axial temperature profile was measured at 4 positions along the sample length at the outside of an alumina ampoule containing the sample. The MSL furnace for the CETSOL samples presented here consisted of a heater and cooling zone separated by an adiabatic zone (Fig. 1). Solidification of the alloys was performed by the controlled displacement of the SQF furnace along the fixed SCA cartridge at a chosen velocity, which can be varied during the experiment. For CETSOL samples 3#1, 3#3 and 3#5 the heater temperatures are constant. The axial

temperature profile was measured at 12 positions along the sample, also at the outside of the crucible containing the sample.

The axial temperature gradients G_L, isotherm velocities v_L, and cooling rates R_L in the samples were calculated from a thermal model of the full furnace in [39], and directly determined from the measurements of the 12 thermocouples in case of the CETSOL samples. The procedures for the determination of the RMIL values and the eutectic fraction f_{eut} is almost identical for SUBSA and CETSOL samples.

Comparing the grain structure of the microgravity samples, all SUBSA samples exhibit shrinkage pores of varying size as well as surface defects [39]. This effect may be attributed to an insufficient function of the spring. In contrast to this inside the CETSOL samples no shrinkage pores were detected, but there was a large surface pore close to the end of solidification stage 2 in samples CETSOL 3#3 and CETSOL3#4 with Al-10 wt.% Cu alloy.

R_{MIL} values and the eutectic fraction f_{eut} could be determined from the longitudinal cross-sections of all processed samples.

All SUBSA microgravity samples (non-refined Al-4wt.%Cu, Al-10wt.%Cu and Al-18wt.%Cu alloys) show a fully equiaxed grain structure. The grain size is largely constant along the sample ($R_{MIL} \approx 1$ mm) with a slight increase in size toward the end of the samples with Al-4wt.%Cu and Al-10wt.%Cu (RMIL ≈ 1.5 mm). This effect was attributed by the original authors to a decreasing cooling rate from about $R_L = 0.07$ K/s to $R_L = 0.04$ K/s. These grain structure can be compared to the grain structure of the CETSOL samples in stage 2 (Table 2). The CETSOL samples 3#1, 3#3 and 3#5 (refined Al-4wt.%Cu, Al-10wt.%Cu and Al- 20wt.%Cu alloys) also show a fully equiaxed grain structure in stage 2. The grain size is constant along the sample ($R_{MIL} = 0.35$ mm – 0.42 mm) for constant cooling rates between $R_L = 0.05$ K/s to $R_L = 0.11$ K/s. Therefore, the cooling rates for SUBSA and CETSOL experiments are comparable, whereas the grain size differs by a factor of approximately three (with the CETSOL experiment exhibiting smaller equiaxed grains). Smaller grains are expected in the CETSOL alloys due to the addition of grain refiner that promotes higher nucleation rates of equiaxed dendritic grains.

In all SUBSA samples (non-refined Al-4wt.%Cu, Al-10wt.%Cu and Al-18wt.%Cu alloys) processed in microgravity a steadily decreasing eutectic percentage feut toward the sample top is shown. This behaviour is explained by the original authors by the existence of a shrinkage-driven flow of solute rich melt that results in a so-called inverse segregation toward the cooled

surface [39]. The top parts of the samples also show more shrinkage pores as the temperature gradient decreased from about G_L = 1.5 K/mm to nearly G_L = 0 K/mm, i.e. as tended towards isothermal solidification conditions. As a consequence of the low axial temperature gradient G_L, in all cases, there was a delay of hundreds of seconds between when the liquidus isotherm reached the end of the sample and when the sample bottom reached the eutectic temperature. During this delay, the mushy zone spanned the entire sample length. This is likely a cause of the significant inverse segregation profile that was observed in all SUBSA samples [39].

The eutectic fraction feut in stage 2 of the CETSOL samples 3#1, 3#3 and 3#5 (refined Al-4wt.%Cu, Al-10wt.%Cu and Al-20wt.%Cu alloys) is practically constant. Also, the temperature gradient in stage 2 was quite constant between G_L = 3.5 K/mm and G_L = 2.5 K/mm. This indicates that there is no shrinkage-driven flow resulting in inverse segregation. Additionally, in the partly melted region (formed during the sample melting phase and present upon starting the solidification experiment) the amount of eutectic fraction was reduced. This can be attributed to the temperature gradient zone melting (TGZM) effect during the thermal homogenization phase before starting the solidification stage 1. This effect was not observed in the SUBSA samples, which were fully melted before starting solidification. This lack of stabilization phase in SUBSA experiments may explain why all experiments exhibit equiaxed microstructures, even for the lowest Al-Cu composition sample.

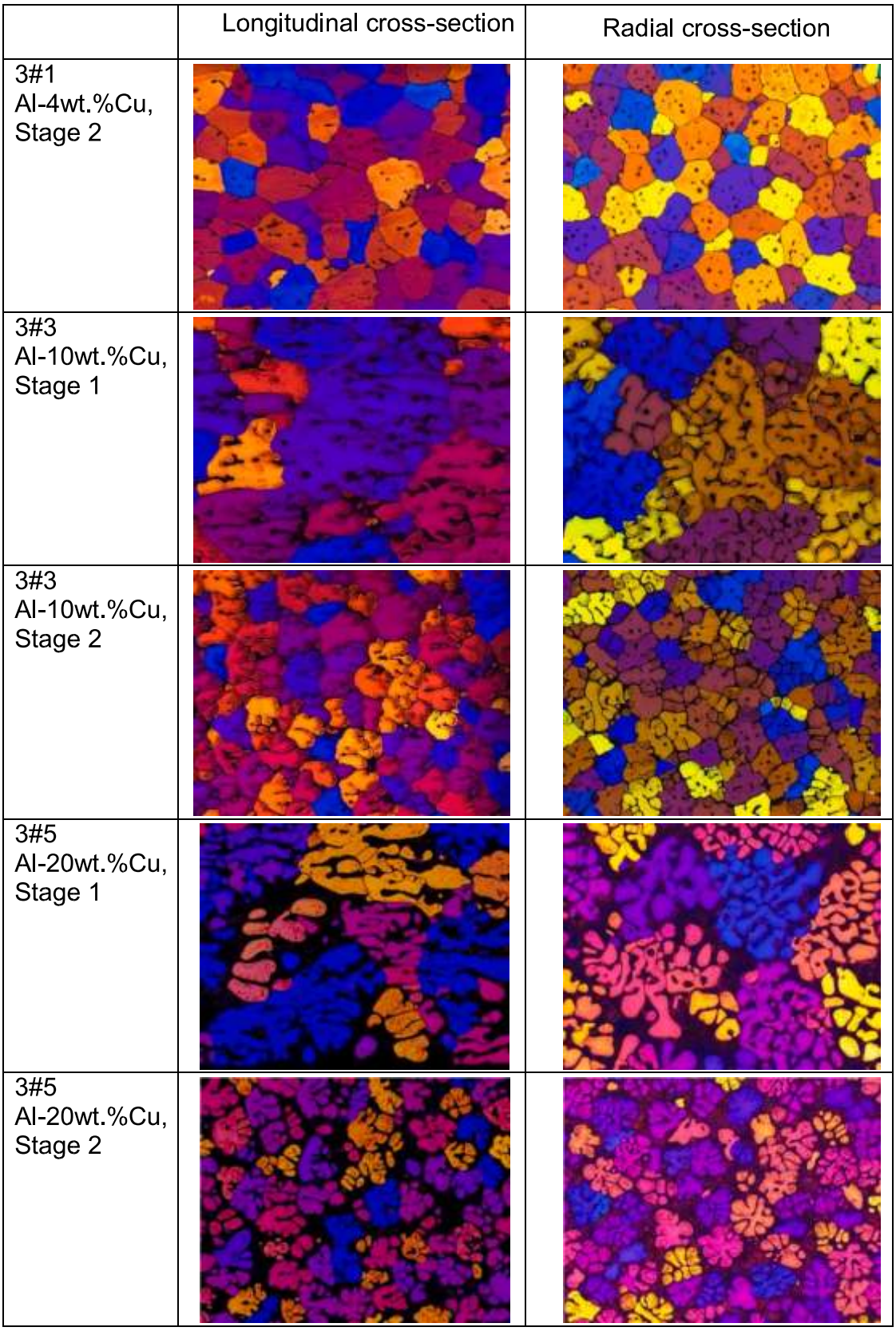

Fig. 11. Selected representative micrographs of the electrolytically etched cross-sections (height x width = 2.10 mm × 2.65 mm) of flight samples CETSOL 3#1, 3#3 and 3#5 showing

the grain structure in longitudinal cross-section (furnace movement from left to right) and in radial cross-section.

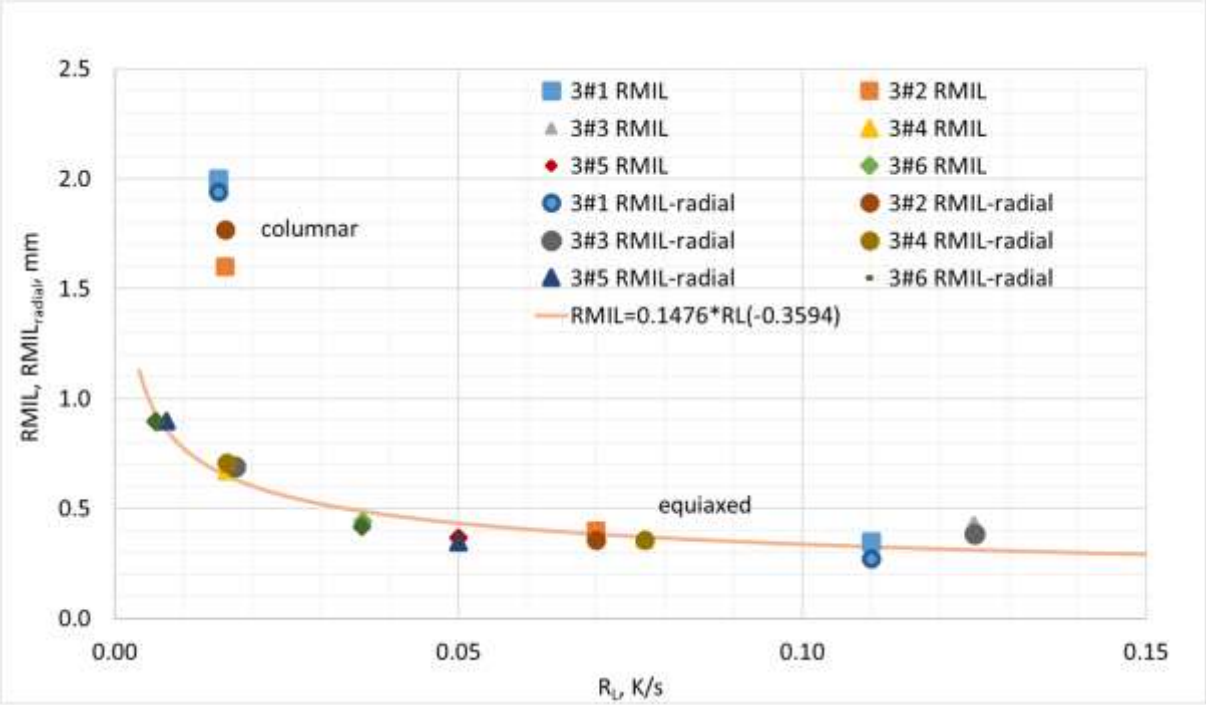

Fig. 12. Steady-state values of RMIL and RMIL radial as a function of RL for the flight samples, determined from radial and longitudinal cross-sections. Also added a fitted curve for the equiaxed values of RMIL and RMIL radial.

6. Conclusion

Benchmark solidification experiments were successfully performed in microgravity on-board the International Space Station ISS within the ESA programme CETSOL. Six cylindrical samples of three refined Al-Cu alloys (Al-4wt.%Cu, Al-10wt.%Cu and Al-20wt.%Cu) were directionally solidified in the gradient furnace MSL. The determination of temperature gradients, interface velocities and cooling rates at liquidus and solidus, and eutectic temperatures provides well-defined thermal boundary conditions.

The analysis of the microstructure in longitudinal cross-sections show dendritic structures without any internal pore formation of pores less than about 10 µm inside the processed alloy and localised surface pores for some samples. The averaged eutectic fraction

f_{eut} is rather constant along the sample with less amount of eutectics in the partly melted region upon starting the solidification experiment.

The samples of refined Al-4wt.%Cu alloy exhibit a sharp CET from columnar grain structure in stage 1 to a fine equiaxed steady-state grain structure in stage 2. This indicates a sharp CET, in contrast to experiments with Al-7wt.%Si alloy, where also progressive CET with elongated grains was observed [12]. This may be attributed to the strong increase of the furnace velocity by a factor of 10, reaching rapidly a fully equiaxed dendritic region. In Al-10wt.% Cu and Al-20wt.% Cu samples, equiaxed dendritic grain growth is observed from stage 1 and the grain size represented by the R_{MIL} value is reduced in stage 2 due to the increase in cooling rate. Detailed analysis of the size of equiaxed grains demonstrates that, despite a qualitative observation of the equiaxed dendrites in longitudinal and radial directions shows some differences in shape, the R_{MIL} and R_{MIL} radial values are comparable. Therefore, equiaxed dendritic growth with negligible elongated dendrites have been obtained in the described experiments.

The evaluation of these microgravity samples demonstrates that no macrosegregation along the sample axis was detected and no radial effects were observed. Therefore, a pure diffusive solidification behavior without any residual melt convection can be assumed for the microgravity experiments, as expected. Compared to directional solidification vertically upwards in 1g for Al-4wt.%Cu alloy, no sedimentation of equiaxed Al-rich dendrites and no floatation of equiaxed dendrites in the melt for Al-20wt.%Cu alloy occured. This is a great advantage for the study of equiaxed grains and columnar front during the CET as mentioned in [28,51] Fragmentation is also expected in the microgravity experiments for Al-10wt.%Cu and Al-20wt.%Cu alloys, but the fragments may not move in the melt because of the absence of buoyancy effects [21,38]. Similar to the findings in Al-7wt.%Si alloys [12] and non-refined Al-Cu alloys [39], it is shown that equiaxed dendritic growth is promoted in microgravity for refined hypoeutectic Al-Cu alloys. For comparable solidification conditions in the microgravity experiments the average grain size RMIL is about a factor three larger for non-refined Al-Cu alloys [39] than for refined alloys. Reference experiments on Earth are in progress to be able to compare with the experiments analysed in the present paper, using alloys which have negatively, neutrally, and positively buoyant primary solid, respectively. The benchmark solidification data reported in this work constitute in themselves benchmark data for modeling of CET and equiaxed dendritic growth.

CRediT authorship contribution statement

G. Zimmermann: Writing – original draft, Investigation, Funding acquisition, Conceptualization. L. Sturz: Investigation. C. Pickmann: Investigation. E. Schaberger-Zimmermann: Investigation. A. Roosz: Investigation. A. R´onaf¨oldi: Investigation. Z. Veres: Investigation. Ch.- A. Gandin: Validation, Investigation. G. Reinhart: Investigation. H. Nguyen-Thi: Validation, Investigation. N. Mangelinck-No¨el: Investigation. Sh. McFadden: Writing – review & editing, Validation. G.-U. Grün: Investigation. W. Sillekens: Investigation.

Declaration of competing interest

The authors declare that they have no known competing financial interests or personal relationships that could have appeared to influence the work reported in this paper.

Acknowledgement

This research work is supported by the European Space Agency under the CETSOL (Columnar to Equiaxed SOLidification processing) ESA MAP project, the CETSOL/HUNGARY ESA PRODEX project (No 4000131880/NL/SH), the French National Space Agency CNES and the German BMWi/DLR under FKZ 50WM2043 and FKZ 50WM2343. The authors acknowledge Hydro Aluminium Rolled Products GmbH, now Speira GmbH, for providing the alloys used in this paper.

References

[1] J.A. Dantzig, M. Rappaz, Solidification, EFPL Press, 2009.

[2] H. Combeau, M. Zaloˇznik, S. Hans, P.E. Richy, Prediction of macrosegregation in steel ingots: influence of the motion and the morphology of equiaxed grains, Metall. Mater. Trans. B 40 (2009) 289–304, https://doi.org/10.1007/s11663-008- 9178-y.

[3] T.-T.-M. Nguyen, Ch.-A. Gandin, H. Combeau, M. Zaloˇznik, M. Bellet, Finite element multi-scale modeling of chemical segregation in steel solidification taking into account the transport of equiaxed grains, Metall. Mater. Trans. A 49 (2018) 1725–1748, https://doi.org/10.1007/s11661-018-4496-4.

[4] R. Jansen, P.R. Sahm, Solidification under microgravity, Mater. Sci. Eng. 65 (1984) 199–212, https://doi.org/10.1016/0025-5416(84)90213-1.

[5] S. Akamatsu, H. Nguyen-Thi, In situ observation of solidification patterns in diffusive conditions, Acta Mater. 108 (2016) 325–346, https://doi.org/10.1016/j.actamat.2016.01.024.

[6] G. Zimmermann, L. Sturz, B. Billia, N. Mangelinck-Noel, H.N. Thi, Ch.-A. Gandin, D.J. Browne, W.U. Mirihanage, Investigation of columnar-to-equiaxed transition in solidification processing of AlSi alloys in microgravity - The CETSOL project, in: A. Meyer, I. Egry (Eds.), International Symposium on Physical Sciences in Space, 2011.

[7] D. Liu, N. Mangelinck-No¨el, Ch.-A. Gandin, G. Zimmermann, L. Sturz, H. Nguyen-Thi, B. Billia, Structures in directionally solidified Al–7wt.% Si alloys: Benchmark experiments under microgravity, Acta Mater. 64 (2014) 253–265.

[8] G. Zimmermann, L. Sturz, H. Nguyen-Thi, N. Mangelinck-Noel, Y.Z. Li, Ch.- A. Gandin, R. Fleurisson, G. Guillemot, S. McFadden, R.P. Mooney, P. Voorhees, A. Roosz, A. Ronafoldi, C. Beckermann, A. Karma, C.H. Chen, N. Warnken, A. Saad, G.U. Grun, M. Grohn, I. Poitrault, T. Pehl, I. Nagy, D. Todt, O. Minster, W. Sillekens, Columnar and equiaxed solidification of Al-7 wt.% Si alloys in reduced gravity in the framework of the CETSOL project, JOM 69 (2017) 1269–1279, https://doi.org/10.1007/s11837-0172397-4.

[9] Y.Z. Li, N. Mangelinck-No¨el, G. Zimmermann, L. Sturz, H. Nguyen-Thi, Effect of solidification conditions and surface pores on the microstructure and columnar-toequiaxed transition in solidification under microgravity, J. Alloy. Compd. 749 (2018) 344–354.

[10] Y.Z. Li, N. Mangelinck-No¨el, H. Nguyen-Thi, G. Zimmermann, L. Sturz, T.J. Cool, E. B. Gulsoy, P.W. Voorhees, Critical parameters concerning the columnar-toequiaxed transition in solidification processing, in: Proceedings of the 6th Decennial International Conference on Solidification Processing, 2017, pp. 317–321. Old Windsor, UK, 25–28 July.

[11] G. Zimmermann, L. Sturz, Y.Z. Li, H. Nguyen-Thi, N. Mangelinck-Noel, R. Fleurisson, G. Guillemot, Ch.-A. Gandin, S. McFadden, R.P. Mooney, P. Voorhees, A. Roosz, C. Beckermann, A. Karma, N. Warnken, E. Perchat, G.- U. Grün, M. Grohn, I. Poitrault, D. Todt, W. Sillekens, Columnar and equiaxed solidification within in the framework of the ESA MAP project CETSOL, in: Proc. 7th International Conference on Solidification and

Gravity 2018, Lillafüred, Hungarian Academy of Sciences, 2018, pp. 17–26. ISBN 978-963-508-8898.

[12] Y.Z. Li, N. Mangelinck-No¨el, G. Zimmermann, L. Sturz, H. Nguyen-Thi, Comparative study of directional solidification of Al-7wt.% Si alloys in Space and on Earth: effects of gravity on dendrite growth and Columnar-to-equiaxed transition, J. Crystal Growth 513 (2019) 20–29.

[13] Y.Z. Li, N. Mangelinck-No¨el, G. Zimmermann, L. Sturz, H. Nguyen-Thi, Modification of the microstructure by rotating magnetic field during the solidification of Al-7 wt.% Si alloy under microgravity, J. Alloy. Compd. 836 (2020) 155458.

[14] A. Ro´osz, A. R´onaf˙oldi, Y. Li, N. Mangelinck-No¨el, G. Zimmermann, H. Nguyen-Thi, M. Sv´eda, Z. Veres, Influence of solidification parameters on the amount of eutectic and secondary arm spacing of Al–7wt.% Si alloy solidified under microgravity, Crystals 12 (2022) 414.

[15] R.P. Mooney, L. Sturz, G. Zimmermann, N. Mangelinck-No¨el, H. Nguyen-Thi, Y. Z. Li, D.J. Browne, S. Fadden, Concurrent model for sharp and progressive columnar to equiaxed transitions validated by directional solidification experiments processed in microgravity conditions, Comput. Mater. Sci. 210 (2022) 111436.

[16] K.Ji Dorari, G. Guillemot, Ch.-A. Gandin, A. Karma, Growth competition between columnar dendritic grains - the role of microstructural length scales, Acta Mater. 223 (2022) 117395.

[17] R. Fleurisson, O. Senninger, G. Guillemot, Ch.-A. Gandin, Hybrid Cellular Automaton - Parabolic Thick Needle model for equiaxed dendritic solidification, J. Mater. Sci. Technol. 124 (2022) 26–40.

[18] D.R. Liu, N. Mangelinck-No¨el, Ch.-A. Gandin, G. Zimmermann, L. Sturz, H. Nguyen Thi, B. Billia, Simulation of directional solidification of refined Al-7 wt%Si alloys - Comparison with benchmark microgravity experiments, Acta Mater. 93 (2015) 24–37.

[19] S. Ganesan, D. Poirier, Densities of aluminum-rich aluminum-copper alloys during solidification, Metall. Mater. Trans. A18 (1987) 721–723.

[20] G. Zimmermann, C. Pickmann, E. Schaberger-Zimmermann, K. Eckert, S. Eckert, Fragmentation in directionally solidified Al-10wt.%Cu alloy at low pulling speeds, in: Proc.

of the 6th Decennial International Conference on Solidification Processes, 2017, pp. 120–123.

[21] G. Zimmermann, C. Pickmann, M. Hamacher, E. Schaberger-Zimmermann, H. Neumann-Heyme, K. Eckert, S. Eckert, Fragmentation-driven grain refinement in directional solidification of AlCu10wt-% alloy at low pulling speeds, Acta Mater. 126 (2017) 236–250.

[22] H. Nguyen-Thi, G. Reinhart, G. Salloum Abou Jaoude, R.H. Mathiesen, G. Zimmermann, Y. Houltz, D. Voss, A. Verga, D.J. Browne, A.G. Murphy, XRMONGF: A novel facility for solidification of metallic alloys with in situ and timeresolved X-ray radiographic characterization in microgravity conditions, J. Crystal Growth 374 (2013) 23–30.

[23] G. Salloum-Abou-Jaoude, H. Nguyen-Thi, G. Reinhart, R.H. Mathiesen, G. Zimmermann, D. Voss, Characterization of motion of dendrite fragment by X-ray radiography on Earth and under microgravity environment, Mater. Sci. Forum 790-791 (2014) 311–316.

[24] G. Reinhart, C.A. Gandin, N. Mangelinck-No¨el, H. Nguyen-Thi, J.E. Spinelli, J. Baruchel, B. Billia, Influence of natural convection during upward directional solidification: a comparison between in situ X-ray radiography and direct simulation of the grain structure, Acta Mater. 61 (13) (2013) 4765–4777.

[25] H. Nguyen-Thi, Y. Dabo, B. Drevet, M.D. Dupouy, D. Camel, B. Billia, J.D. Hunt, A. Chilton, Directional solidification of Al-1.5wt% Ni alloys under diffusion transport in space and fluid flow localisation on Earth, J. Crystal Growth 281 (2005) 654–668.

[26] A.G. Murphy, W. Mirihanage, D.J. Browne, R.H. Mathiesen, Equiaxed dendritic solidification and grain refiner potency characterised through in situ Xradiography, Acta Mater. 95 (2015) 83–89.

[27] L. Abou-Khalil, G. Salloum-Abou-Jaoude, G. Reinhart, C. Pickmann, G. Zimmermann, H. NguyenThi, Influence of gravity level on Columnar-to- Equiaxed Transition during directional solidification of Al - 20 wt.% Cu alloys, Acta Mater. 110 (2016) 44–52.

[28] F. Ngomesse, G. Reinhart, H. Soltani, G. Zimmermann, D.J. Browne, W. Sillekens, H. Nguyen-Thi, In situ investigation of the Columnar-to-Equiaxed Transition during directional solidification of Al20wt.%Cu alloys on Earth and in Microgravity, Acta Mater. 221 (2021) 11740124.

[29] G. Reinhart, Ch.-A. Gandin, N. Mangelinck-Noel, H. Nguyen-Thi, J.-E. Spinelli, J. Baruchel, B. Billia, Influence of natural convection during upward directional solidification: a comparison between in situ Xray radiography and direct simulation of the grain structure, Acta. Mater. 61 (2013) 4765–4777.

[30] H. Soltani, F. Ngomesse, G. Reinhart, M.C. Benoudia, M. Zahzouh, H. Nguyen-Thi, Impact of gravity on directional solidification of refined Al-20wt.%Cu alloy investigated by in situ X-radiography, J. Alloys Compd. 862 (2021) 158028.

[31] W.U. Mirihanage, H. Dai, H. Dong, D.J. Browne, Computational modeling of columnar to equiaxed transition in alloy solidification, Adv. Eng. Mater. 15 (2013) 216–229.

[32] A.G. Murphy, R.H. Mathiesen, Y. Houltz, J. Li, C. Lockowandt, K.J. Henriksson, G. Zimmermann, A. Verga, D.J. Browne, XRMON-SOL: isothermal equiaxed solidification of a grain refined Al-20wt.%Cu alloy, J. Crystal Growth 440 (2016) 38–46.

[33] A.G. Murphy, R.H. Mathiesen, Y. Houltz, J. Li, C. Lockowandt, K. Henriksson, N. Melville, D.J. Browne, Direct observation of spatially isothermal equiaxed solidification of an Al–Cu alloy in microgravity onboard the MASER13 sounding rocket, J. Crystal Growth 454 (2016) 96–104.

[34] A. Olmedilla, M. Zaloˇznik, H. Combeau, Quantitative 3D mesoscopic modeling of grain interactions during equiaxed dendritic solidification in a thin sample, Acta Mater. 173 (2019) 249–261.

[35] J. Mullen, M. Celikin, D.J. Browne, Quantification of the impact of gravity on isothermal equiaxed alloy solidification using machine learning, in: 72nd International Astronautical Congress, IAC 2021, 2021 (IAC,).

[36] F. Kargl, J. Drescher, C. Dreißigacker, M. Balter, M. Becker, M. Wegener, E. Sondermann, XRISEM: X-radiography facility for solidification and diffusion studies of alloys aboard sounding rockets, Rev. Sci. Instrum. 91 (2020) 013906.

[37] M. Becker, M. Kolbe, S. Steinbach, F. Kargl, Surface boundary-dendrite interactions in thin metallic Al-alloy samples, Scr. Mater. 209 (2022) 114386.

[38] G. Reinhart, D.J. Browne, F. Kargl, F. García-Moreno, M. Becker, E. Sondermann, K. Binder, J.S. Mullen, G. Zimmermann, R.H. Mathiesen, W. Sillekens, H. Nguyen- Thi, In-

situ X-ray monitoring of solidification and related processes of metal alloys, npj Microgravity 9 (2023) 70, https://doi.org/10.1038/s41526-023-00321-z.

[39] T.J. Williams, C. Beckermann, Benchmark Al-Cu solidification experiments in microgravity and on earth, Met. Mater. Trans. 54A (2023) 405–422.

[40] Ch.-A. Gandin, B. Billia, G. Zimmermann, D. Browne, M.-D. Dupouy, Columnar-oequiaxed transition in solidification processing: a project of the European space agency - microgravity applications promotion program, solidification and gravity IV - 2004, Mater. Sci. Forum 508 (2006) 393–404.

[41] B. Billia, Ch.A. Gandin, G. Zimmermann, D. Browne, M.D. Dupouy, Columnar equiaxed transition in solidification processing: the ESA-MAP CETSOL project, Microgravity Sci. Technol. 16 (2005) 20–24.

[42] E. Schaberger, F. Grote, A. Schievenbusch, Farb¨atzung und Farbbildanalyse – Ein Weg zur Charakterisierung von Gefügen innovativer Gusswerkstoffe, Prakt. Metallographie 37 (2000) 419–434.

[43] O. Zobac, A. Kroupa, A. Zemanova, K.W. Richter, Experimental description of the Al-Cu binary phase diagram, Metall Mater. Trans. A 50 (2019) 3805–3815, https://doi.org/10.1007/s11661-019-05286-x.

[44] Thermo-Calc Software: Computational Materials Engineering; https://thermocalc.com.

[45] A. Ro´osz, A. R´onaf¨oldi, Y.Z Li, N. Mangelinck-No¨el, G. Zimmermann, H. Nguyen-Thi, M. Sv´eda, Zs. Veres, Influence of solidification parameters on the amount of eutectic and secondary arm spacing of Al–7wt.% Si alloy solidified under microgravity, Crystals 12 (1-18) (2022) 414.

[46] H. Nguyen Thi, B. Drevet, J.M. Debierre, D. Camel, Y. Dabo, B. Billia, Pr´eparation of the initial solid - liquid interface and melt in directional solidification, J. Crystal Growth 253 (2003) 539–548.

[47] H. Nguyen-Thi, G. Reinhart, A. Buffet, T. Schenk, N. Mangelinck, H. Jung, N. Bergeon, B. Billia, H. H¨artwig, J. Baruchel, In situ and Real-time analysis of TGZM phenomena by synchrotron X-ray radiography, J. Crystal Growth 310 (2008) 2906–2914.

[48] A.B. Phillion, M. Zaloznik, I. Spindler, N. Pinter, C.A. Aledo, G. Salloum-Abou- Jaoude, G.Reinhart H.Nguyen-Thi, G. Boussinot, M. Apel, H. Combeau, Evolution of a mushy zone

in a static temperature gradient using a volume average approach, Acta Mater. 141 (2017) 206–216.

[49] H. Soltani, G. Reinhart, M.C. Benoudia, F. Ngomesse, M. Zahzouh, H. Nguyen-Thi, Equiaxed grain structure formation during directional solidification of a refined Al-20wt.%Cu alloy: in situ analysis of temperature gradient effects, J. Crystal Growth 587 (2022) 126645.

[50] D. Eskin, Q. Du, D. Ruvalcaba, L. Katgerman, Experimental study of structure formation in binary Al-Cu alloys at different cooling rates, Mater. Sci. Eng. A405 (2005) 1–10.

[51] L. Abou-Khalil, Z. Thompson, G. Reinhart, T. Stan, L. Sturz, G. Zimmermann, P. W. Voorhees, N. Mangelinck-No¨el, H. Nguyen-Thi, Three-dimensional investigation of fragment distribution in Al-7wt.% Si solidified in microgravity, Acta Mater. 250 (2023) 8.